The Effects of Basin Slope and Boundary Friction on the Character and Plunge Location of Hyperpycnal Flows Entering a Laterally Unbounded Basin

Shantanu V. Bhide

Thesis submitted to the Faculty of the
Virginia Polytechnic Institute and State University
in partial fulfillment of the requirements for the degree of

Master of Science
in
Environmental Engineering

Kyle B Strom, Chair
Randel L Dymond
Durelle T Scott

April 9, 2019
Blacksburg, Virginia

Keywords: Plunging, Hyperpycnal Flows, Laterally Unconfined Basin

The Effects of Basin Slope and Boundary Friction on the Character and Plunge Location of Hyperpycnal Flows Entering a Laterally Unbounded Basin

Shantanu V. Bhide

(ABSTRACT)

This thesis focuses on the behaviour of hyperpycnal plumes in river mouth discharges. The plunging of high density flows in two dimensional channels has been extensively studied before. A fundamental assumption in these studies is that the flow is laterally confined. These studies allow the flow to plunge only in two directions, the horizontal x-direction and the vertical z-direction. The goal of this study is to determine if there is observable plunging of hyperpycnal flows in the lateral y-direction, i.e. lateral spreading, in a three dimensional domain and to find out the parameters influencing the lateral spread. Previous studies conducted in laterally confined channels suggest that hyperpycnal flows plunge when the flow reaches a densimetric Froude number of unity. This study attempts to find the densimetric Froude number at hyperpycnal plunging in a three dimensional domain and if it is influenced by the factors that also influence the spread. This study also analyzes whether the cross-shore location for plunging changes when lateral spreading is accounted for, relative to a two dimensional analysis and if the plunging is limited to flow reaching a certain depth. This was accomplished through a series of experimental simulations on a hypothetical river mouth domain using Delft-3D, a hydrodynamic modeling software. Three parameters viz. the bottom slope of the receiving basin, the bottom friction and the density difference between inflow and ambient liquid were varied to test their influence on the plume spread rate.

The Effects of Basin Slope and Boundary Friction on the Character and Plunge Location of Hyperpycnal Flows Entering a Laterally Unbounded Basin

Shantanu V. Bhide

(GENERAL AUDIENCE ABSTRACT)

It is crucial for researchers to have the expertise in modeling flow processes that develop in oceans, lakes and reservoirs in order to aid efforts in improving conditions for water quality within such domains. Hyperpycnal flows, also commonly known as high density flows are among one of the the less studied phenomenon in this discipline. This phenomenon occurs when a river carrying water with high density flows into an ocean, lake or a reservoir containing water with a lower density. Such flow regimes cause the inflow to submerge and sink to the bottom (plunge) and form a density current on the bed of the receiving basin. Studying density flows is important to model the transport of sediments, dissolved solids or pollutants. This study aims to improve the existing understanding of hyperpycnal plumes, their plunge location and spread in a three dimensional domain. For this, a simulation software Delft3D was used to build a model that is representative of the system and closely resembles the flow processes taking place in the aforementioned domains. Simulations were then run to collect data on how factors like the initial flow conditions ($\Delta\rho$), the basin slope (S) and friction (Chézy coefficient, C_z) have an impact on the phenomenon. This data was then compared to previous analyses to show the difference in plume behaviour and prediction of plunging. This study serves as a stepping stone in the ultimate goal of developing a prediction model for hyperpycnal plumes, indicating that Delft3D is a promising tool for analyzing such phenomenon.

Dedication

I dedicate this thesis to my family, my pillars of strength and thank them for their endless support, love and care.

Acknowledgments

I would like to express my sincere appreciation to my advisor Dr. Kyle Strom for being a great mentor and for his assistance, continuous support and trust in my research work. I would also like to thank my other advisory committee members, Dr. Randell Dymond and Dr. Durelle Scott, for taking time out to serve on my committee and showing me different perspectives regarding my study. Additionally, I would like to thank my fellow graduate students Amit Naik and Deepika Mulchandani for their help in answering my python queries. I would also like to thank Jeff Culp, Brandon Dillon and Dr. Oral Yagci for being great colleagues in the lab and for engaging in productive discussions with me. Last but not the least, I would like to thank my parents and my sister for their love, encouragement and continuous support.

Contents

List of Figures

List of Tables

List of Symbols and Abbreviations

γ	Mixing coefficient
ρ_a	Ambient water density (kg/m^3)
ρ_m	Inflow density (kg/m^3)
A	Cross sectional area (m^2)
b	Channel width (m)
C_z	Chézy friction coefficient
Fr_d	Densimetric Froude number
g	Standard acceleration due to gravity (m/s^2)
g'	Reduced acceleration due to gravity (m/s^2)
h	Flow depth (m)
h_p	Plunge depth (m)
R_i	Richardson number
U	Flow velocity (m/s)
W	Plume width (m)
xp	Plunge location along x direction
xp_i	Incipient plunge location along x direction

ppt	Parts per thousand
ROMS	Regional Ocean Modeling System

Chapter 1

Introduction

1.1 Overview

Rivers are the primary conduits for delivery of terrigenous sediment and organic matter to lakes, reservoirs, and ultimately our ocean basins (Strom and Keyvani, 2016). This is visually evident when sediment-laden rivers enter larger receiving basins, producing sediment plumes as seen in Figure 1.1. The sediment and organic material from such plumes may deposit and be preserved in deltaic zones, or may be carried and mixed by currents to deposit elsewhere on the continental shelf or ocean or lake basin. Both of these outcomes are governed in large part by the transport and depositional mechanics of the river discharge and the strength of local currents. A knowledge of the transport and depositional mechanics of river mouth discharges is therefore important for understanding deltaic processes such as land building and for understanding the fate and packaging of sediments and organic material in basins.

The broad context for the transport and depositional mechanics of river mouth discharges is set by the density difference between the river and the larger receiving basin. Density, ρ, in both bodies of water is primarily set by the temperature of the water (T), the amount of dissolved salts (here quantified with salinity, S, in parts per thousand (ppt)), and the amount of suspended particulates in the water column (quantified as a concentration, C): $\rho = \rho(T, S, C)$.

If the density of the receiving water body (ρ_a) is greater than the density of the river discharge (ρ), then the river discharge dynamics will be influenced by positive buoyant forces.

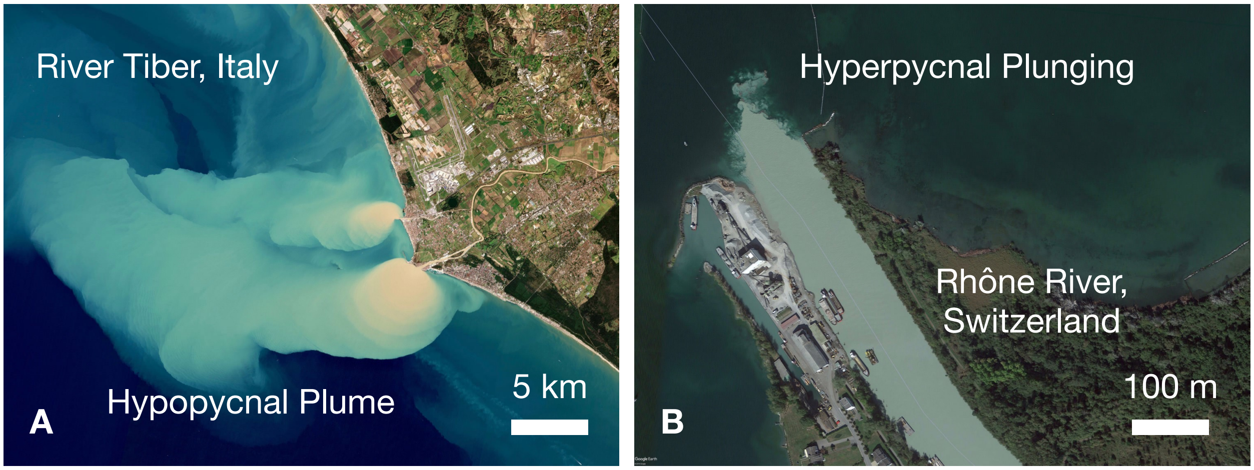

Figure 1.1: Examples of sediment-laden river plumes. (A) The positively buoyant (hypopycnal) plume of the River Tiber on the western coast of Italy on 5 February 2019; image captured by the European Space Agency's Copernicus Sentinel-2B satellite (`https://www.esa.int/spaceinimages/Images/2019/02/Sediment_plume_at_sea`). (B) The negatively buoyant (hyperpycnal) Rhône River plunging into Lake Geneva, Switzerland; image taken from Google Earth (image date: September 27, 2018, location: 46°23'44.18" N 6°51'39.89" E)

Such discharges are referred to as "hypopycnal" discharges. A classic example of this type of flow is when freshwater rivers meet salty oceans. In such cases, the positively buoyant freshwater discharge will push the saltwater basinward until there is a balance between the dynamic and hydrostatic freshwater and saltwater forces at the bed. At this point the freshwater flow will detached from the boundary and loft over the more dense saline water (Geyer et al., 2004) (Fig. 1.1A). This lift off typically occurs at a critical densimetric Froude number of about 1 (Geyer et al., 2004). The densimetric Froude number, Fr_d, represents the ratio of the rivers inertial forces over the gravitational forces induced by the density difference. Or said another way, as the ratio of the average velocity over the celerity of the internal wave or gravity front. The densimetric Froude number is given by:

$$Fr_d = \frac{U}{\sqrt{g'h}} \tag{1.1}$$

where U is the average flow velocity, g' is the apparent reduced acceleration of gravity for the less dense fluid, $g' = g(\rho_a - \rho)/\rho$, and h is the flow depth. The same basic properties can also be expressed in the bulk Richardson number:

$$R_i = \frac{g'h}{U^2} = \frac{1}{Fr_d^2} \tag{1.2}$$

Following lift off, and upon entering the laterally unconfined basin, the plume will spread out laterally due to momentum diffusion and the difference in the plume and ambient fluid density at the edges of the plume (Wright and Coleman, 1974; Hetland and MacDonald, 2008). Of these two spreading mechanisms, buoyancy dominates. As a result, the rate of width expansion, dW/dx, is set by the internal wave speed of the stratified front, $\sqrt{g'h}$ (Hetland and MacDonald, 2008; Hetland, 2010):

$$\frac{dW}{dx} = 2Fr_d^{-1} = 2\sqrt{Ri} \tag{1.3}$$

For this case, the speed at which sediment is removed from the surface plume towards the bed is thought to scale with the settling velocity of the individual or flocculated particles in the plume (figure 1.2).

The second broad class of river mouth discharges are those for which the incoming river density is greater than that in the receiving basin, $\rho > \rho_a$. Such flows are referred to as “hyperpycnal” flows (Mulder and Syvitski, 1995; Bhattacharya and MacEachern, 2009). The increased density in the inflow can be the result of cooler temperatures, increased salt levels, or large volumes of suspended sediment. In any case, if the density difference is great enough, the negative buoyant forces associated with the inflow can result in bulk plunging of the entire river (Akiyama and Stefan, 1984; Lamb and Mohrig, 2009), to create a river fed gravity or turbidity current (figure 1.2). Such gravity driven underflows can transport

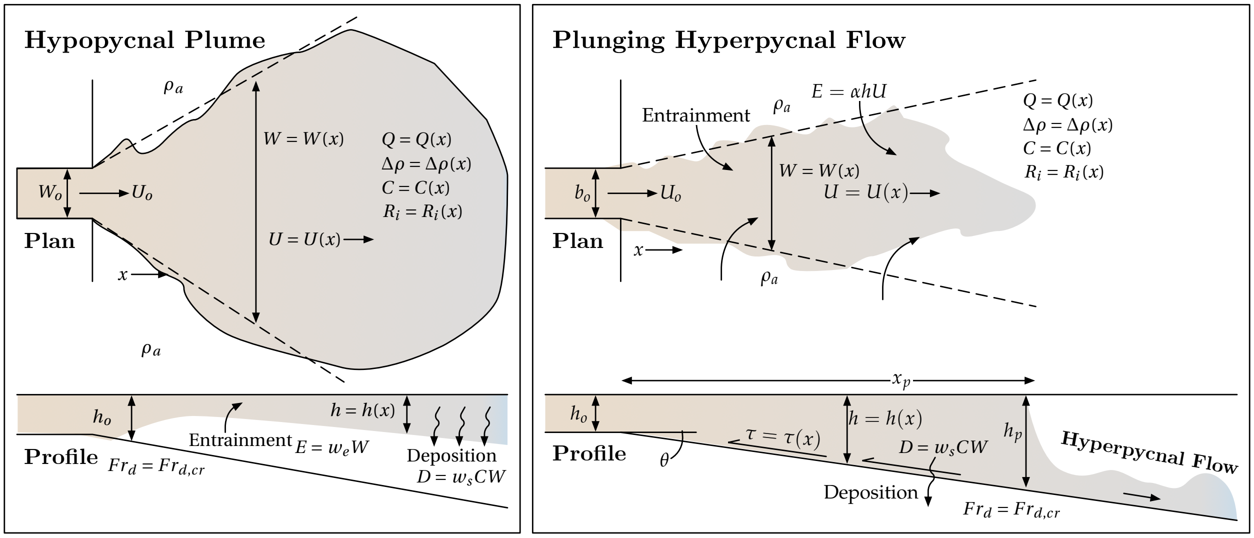

Figure 1.2: Conceptual sketches of hypopycnal (left) and hyperpycnal (right) rivers discharging into a laterally unbounded basin filled with water of density, ρ_a.

river water and sediment significant distances out into the basin if slopes are high enough (Wright and Friedrichs, 2006), or they can result in rapid deposition in the deltaic zone on lower slopes. In the case of rivers entering lakes and reservoirs, it is often the combination of cooler water and suspended sediment in the river that lead to plunging; the Rhône River entering Lake Geneva is a prime example of a hyperpycnal flow driven by cool, sediment laden river water (figure 1.1B). In the case of a river entering the ocean, the excess density in the inflow has to come from suspended sediment since the clearwater density of the river is always less than that of the salty ocean. In fact, the on-average 35 ppt difference between fresh and salt water (a difference of roughly 25 kg/m^3) means that a river needs to carry approximately 40 g/l of sediment or more to go hyperpycnal in coastal settings. Such extreme suspended sediment concentrations do occur in rivers on active margins (Warrick and Milliman, 2003; Milliman et al., 2007; Warrick et al., 2008; Wang et al., 2010). However, their occurrence is rare (Mulder and Syvitski, 1995). This means that hyperpycnal processes are of more interest in lakes and reservoirs, or possibly in paleo-environments where ocean salinity was lower.

This thesis deals with both hypo- and hyperpycnal river-mouth discharges into quiescent receiving basins. However, the focus of the work is on hyperpycnal flows.

1.2 Hyperpycnal Flows and the Plunge Point

Hyperpycnal flows can be broken up into three conceptual zones or reaches as shown in Figure 1.3. Zone 1 is the laterally confined region of the river leading up to the mouth. Zone 2 is the region that extends from the river mouth up to the start of the plunge point, and Zone 3 is the subaqueous density current that forms downstream of the plunge point. One can therefore think of the plunge point as the transition region from the inertially-dominated river-mouth jet to the buoyancy-dominated gravity flow downstream. Depending on conditions, plunging can happen either within the channel or after the river has entered the laterally unconfined basin. The paper of Alavian et al. (1992) does a good job of explaining these different zones and many of the factors important in the dynamics of each within the context of a dense saline flow.

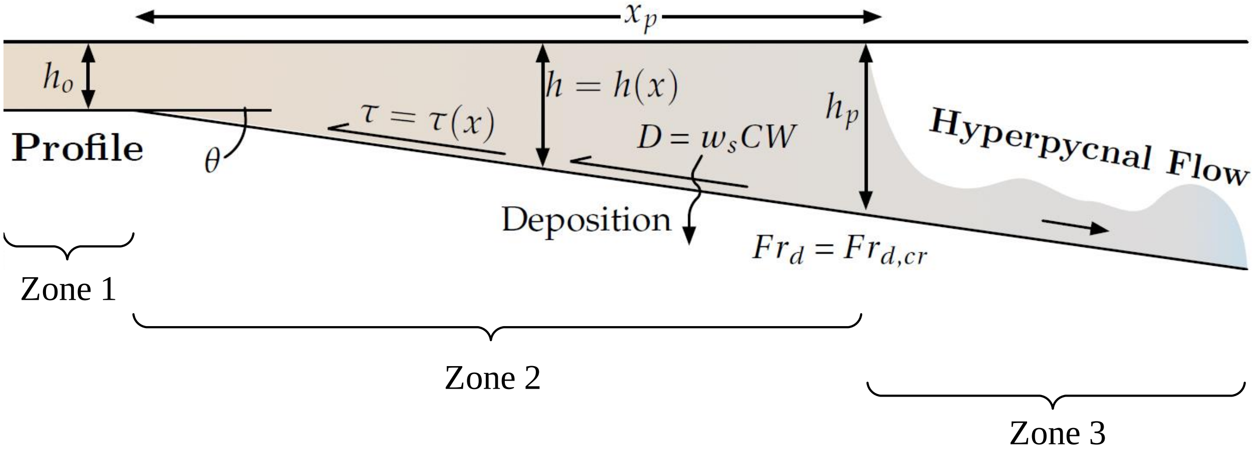

Figure 1.3: Conceptual zones in hyperpycnal flows.

Some of the studies on hyperpycnal flows are particularly interested in the nature of the density current in Zone 3 (e.g., Alavian, 1986; Khan et al., 2005; Chen et al., 2013). In this thesis I focus on a different part of the flow; namely, the conditions associated with plunging and the effect of different flow and basin properties on the location of the plunge point.

Key questions of interest with respect to hyperpycnal plunging include the following: what are the necessary conditions for plunging to occur?, where does plunging occur?, and, how much ambient fluid is entrained before and during plunging?. These questions are important because it has been shown that having higher density in the inflow than the receiving basin is not a sufficient criteria to predict whether or not plunging will occur (e.g., Lamb et al., 2010), and because knowing how much the flow has been diluted by the time it gets to the beginning of Zone 3 is important for predicting the dynamics of the downstsream density current (e.g., Fang and Stefan, 1991).

Whether or not a current plunges is important for knowing how sediment moves through and deposits in a reservoir (e.g., Yu et al., 2000). For example, if a flow does not plunge, then most of the sediment will be deposited in the region proximal to the delta. However, if plunging does occur, the turbidity current can move sediment much further out into the reservoir, even to the point of clogging intake structures on or near the dam (Wang et al., 2018). Therefore knowing whether or not a flow of a particular discharge, temperature, and sediment concentration will plunge or not is useful information for reservoir sediment management and dam operation. Furthermore, being able to know the conditions that cause plunging can be helpful in interpreting the depositional context from the sedimentary record (Nakajima, 2006; Milliman et al., 2007; Bhattacharya and MacEachern, 2009; Lamb and Mohrig, 2009; Lamb et al., 2010; Olariu et al., 2012). The sedimentary deposits from hypopycnal plumes and hyperpycnal flows have different vertical and longitudinal structure (Bhattacharya and MacEachern, 2009). Therefore, if the sedimentary record contains deposits that appear to be associated with hyperpycnal flows, then such deposits could be used to help constrain the flow, temperature, salinity, and sediment loading conditions that must have existed at the time of deposition. The broad goal of research in this thesis is to advance our ability to define the conditions that lead to plunging in the case of a laterally confined river entering a larger receiving basin.

The majority of previous work on plunging has been carried out within the context of a laterally confined channel. For example, several studies have looked to answer the question, ”what are the plunge conditions in a channel of constant width and linearly varying depth?” This particular problem has been studied analytically (Singh and Shah, 1971; Savage and Brimberg, 1975; Akiyama and Stefan, 1984; Parker and Toniolo, 2007; Dai and Garcia, 2010), experimentally (Singh and Shah, 1971; Johnson and Stefan, 1988; Lee and Yu, 1997; Arita and Nakai, 2008), and numerically (Farrell and Stefan, 1988; Bournet et al., 1999; Kassem and Imran, 2001; dong An and Li, 2010; Schuch et al., 2018). Plunging in diverging channels has also been investigated experimentally and numerically (e.g., Johnson et al., 1987; Akiyama and Stefan, 1987; Stefan and Johnson, 1989; Kassem et al., 2003; Üneş, 2008), though the theory surrounding this problem is not as well understood. Even less well studied is the case of a channel entering a laterally unbounded basin. Several studies have looked at hypopycnal flows in this setting (e.g., Wright and Coleman, 1974; Hetland and MacDonald, 2008; Yuan and Horner-Devine, 2013), but few studies on hyperpycnal flows have been conducted; the exceptions to this are the studies of Hauenstein and Dracos (1984), Chen et al. (2013), and Tseng and Chou (2018).

One consistent outcome from the body of work on plunging in both laterally confined channels and unconfined basins is that plunging first occurs at some location basinward of its final position. After initial plunging, the plunge location then retreats landward before locking into its steady-state location at $x = x_p$ (figure 1.2), as long as inflow conditions remain constant (Tseng and Chou, 2018). At the steady state condition, most studies have sought to characterize the conditions at plunging with a characteristic or critical densimetric Froude number. That is, at plunging, $Fr_d = Fr_{d,cr}$ (e.g., Akiyama and Stefan, 1984; Hauenstein and

Dracos, 1984; Parker and Toniolo, 2007). This makes sense as Fr_d represents the ratio of the inertial to buoyant driving forces (equation 1.1). Nevertheless, plunging has not always been found to form at a single Fr_d value. Instead, Fr_d at plunging, $Fr_{d,cr}$, as been reported to range between 0.3 to 1.72 depending on the dimensionality of the domain and the conditions the studies were conducted in. A summary of reported $Fr_{d,cr}$ values are given in table 1.1. Overall, the Fr_d value at plunging tends to be more tightly constrained in laterally bounded 2D channel flows (with average $Fr_{d,cr}$ values of about 0.7 to 1).

Study	Critical Fr_d	Domain	Study Type
Ford and Johnson (1980)	$0.1 \sim 0.7$	2D channel, laterally confined	Analytic
Itakura and Kishi (1979)	$0.54 \sim 0.69$	2D channel, laterally confined	Analytic
Singh and Shah (1971)	$0.3 \sim 0.8$	2D channel, laterally confined	Experimental
Kan and Tamai (1981)	$0.45 \sim 0.92$	2D channel, laterally confined	Analytic
Fukuoka et al. (1980)	$0.37 \sim 0.72$	2D channel, laterally confined	Experimental
Farrel and Stefan (1986)	$0.66 \sim 0.7$	2D channel, laterally confined	Numerical
Akiyama and Stefan (1987)	$0.56 \sim 0.89$	Diverging Channel	Experimental
Lee and Yu (1997)	$0.6 \sim 1$	2D channel, laterally confined	Experimental
Dai and Garcia (2010)	$0.3 \sim 0.6$	2D channel, laterally confined	Analytic
Parker and Toniolo (2007)	$0.5 \sim 1$	2D channel, laterally confined	Analytic
Lamb et al. (2010)	$0.45 \sim 1$	2D channel, laterally confined	Experimental
Tseng and Chou (2018)	$0.64 \sim 1.72$	Unconfined	Numerical

Table 1.1: Reported critical Fr_d at the plunge point.

The idea of a critical densimetric Froude number has led, at least in the laterally-confined plunge scenario, to a two-fold criteria for plunging in hyperpycnal flows. The first criteria is simply that the density of the inflow must be higher than the density of the ambient, $\rho > \rho_a$. The second is the need for sufficient water depth, often refereed to as the plunge depth (h_p), to reduce the densimetric Froude number below the critical value for plunging. For example, in a 2D channel with no entrainment, the discharge in the channel is constant and the velocity varies linearly with depth: $U = q/h$, where q is the unit width discharge and h is the depth of the channel, which can vary with x. Replacing U with q/h

and solving for h in the Froude number definition (equation 1.1) results in:

$$h_p = \left(\frac{q}{Fr_{d,cr}\sqrt{g'}} \right)^{2/3} \tag{1.4}$$

An implication of a critical depth required for plunging is that the topography of the receiving basin, and in some cases even the settling properties of the sediment, can limit plunging even if $\rho > \rho_a$. These ideas are discussed in detail in Lamb et al. (2010).

If a river is denser than the receiving body of water, and plunging did not occur within the confined channel region (Zone 1), then the densimetric Froude number of a river at the river mouth $Fr_{d,0}$ must be greater than $Fr_{d,cr}$. As it turns out, this is often the case. This means that plunging will occur in the basin and not in the laterally confined channel. Following equation 1.4 and the 2D channel theory (no spreading or entrainment of ambient fluid up to the point of plunging), the plunge location could be estimated from the basin topography and by allowing g' to change due to sediment settling Lamb et al. (2010). However, this analysis neglects the effects of lateral spreading of the discharge in Zone 2 and does not account for entrainment of ambient fluid that may occur across the sides of the discharge once it enters the basin (figure 1.2). In fact, a 2D analysis using equation 1.4 would suggest that plunging can never occur if a flow with $\rho > \rho_a$ and $Fr_{d,0} > Fr_{d,cr}$ enters a horizontal basin. However, in an laterally unbounded domain, the discharge is free to expand laterally and ambient fluid can entrain across the sides of the flow. Lateral spreading of the plume (through momentum diffusion and possibly buoyant spreading similar to the hypopycnal case) and entrainment of ambient fluid should all lead to a reduction in the overall velocity of the plume while entrainment will produce a decrease in g'. Therefore, one might expect that plunging could occur even if the basin slope was zero.

If plunging does indeed occur around some critical Fr_d value, then developing a simple method to evaluate the conditions at the river mouth that could lead to plunging in a laterally unbounded domain, similar to what was done by Lamb et al. (2010) for the bounded domain, could be a useful tool. One possible way to do this would be to use 1D integral jet/plume equations to evaluate the transformation in the cross-sectionally averaged variables of $Q = Q(x)$, $W = W(x)$, $U = U(x)$, $\Delta\rho = \Delta\rho(x)$ (and therefore $Fr_d = Fr_d(x)$) from the river mouth basinward. Attempts to do so have been reasonably successful for the case of discharges emanating from engineering-scale slot jets with relatively small width to depth ratios at the river mouth ($W_o/h_o \sim 0.5$ to 1.8) (Fang and Stefan, 2000; Strom and Bhattacharya, 2012). However, application of those same equations to geophysical-scale aspect ratios ($W_o/h_o \sim 10$ to 100) leads to a lateral contraction of the discharge upon leaving the river mouth and a delay in plunging. In fact, for steep basins, the 2D criteria for plunging (equation 1.4) predicts plunging at locations landward of the integral jet/plume analysis. The physicality of this outcome is suspect as diffusion of momentum, and possibly lateral buoyant spreading, should cause the river width to expand upon leaving the mouth.

1.3 Research Questions

Hyperpycnal plunging in laterally unbounded basins has been observed and explored in the field (figure 1.1B), laboratory (Hauenstein and Dracos, 1984; Johnson and Stefan, 1988), and through numerical simulations (Chen et al., 2013; Tseng and Chou, 2018). Most of these studies show that plunging happens soon upon exit from the mouth. Yet little information has been collected on the nature of the flow between the mouth and the plunge location (over Zone 2), and it remains unknown whether or not a critical Fr_d value can predict plunging. If such a condition exists, it seems reasonable that integral jet/plume models could be used as a computationally inexpensive method for assessing if and where a discharge will plunge in an unbounded domain. Yet using the equations designed for engineering-scale river-mouth aspect ratios, $W_o/h_o \sim 1$, in geophysical settings produces unreasonable results. The equations used to produce buoyant spreading in hypopycnal plumes with geophysical-scale aspect ratios (equation 1.3), can be used in the integral equations setup for a hyperpycnal flow. But it remains unclear whether or not the model can actually describes spreading the hyperpycnal case.

The focus of this research is on plunging of hyperpycnal flows in a laterally unconfined receiving basin. The work seeks to understand how basin slope, bottom friction, and initial density difference affect the nature of the flow up to the point of plunging (i.e., in Zone 2), and to identify the specific conditions at the plunge point. One of the primary questions the work addresses is whether the discharge spreads laterally in Zone 2. And, if so, what are the factors influencing the spread rate. This primary goal is broken up below into four research questions and associated hypotheses to help guide the experimental development and data interpretation. The sub-questions this study seeks to answer are:

Research Question 1: Does lateral spreading of a river mouth discharge occur between the mouth and the plunge point for conditions at the mouth of $\rho > \rho_a$ and $Fr_{d,0} > Fr_{d,cr}$? **Hypothesis:** Spreading does occur, and the spread changes the cross shore location for plunging relative to a two dimensional, depth limited plume. **Rational:** In a three dimensional domain, as the plume enters the receiving basin, it begins to spread in the direction parallel to the shore due to momentum diffusion and lateral buoyant spreading.

Research Question 2: How does the basin slope (S), bottom friction (C_z), and initial density difference ($\Delta\rho$) affect plume spreading and plunge location? **Hypothesis:** Spread rate decreases with increasing slope, increasing friction, and decreasing density difference. **Rational:** Decreasing basin slope and increasing friction both serve to impede the flow in the primary direction of flow (basinward). As a result, basins with lower slopes and higher boundary friction will tend to produce plumes that spread at a higher rate. Increasing density differences should increase the rate of spread if lateral buoyant spreading is a factor in the spread rate (equation 1.3).

Research Question 3: Is spreading in Zone 2 controlled primarily by momentum diffusion or buoyancy? **Hypothesis:** Lateral buoyant spreading occurs in Zone 2 of a hyperpycnal discharge, and the rate of spread is similar to that in a hypopycnal plume (equation 1.3). **Rational:** Differences in the hydrostatic forces between the current and ambient flow will add a lateral velocity component that can be superimposed upon the primary basinward direction of the flow. As with the positively buoyant case, the negatively buoyant flow's lateral velocity will be set by the spread of the internal wave between the flow and ambient $\sqrt{g'h}$.

Research Question 4: What is the densimetric Froude number at plunging? Is there a single critical value? Is it influenced by the same factors that influence spread? **Hypothesis:** Plunging of hyperpycnal flows occurs when the flow reaches a densimetric Froude number around 1. **Rational:** Studies by Akiyama and Stefan (1987), Lee and Yu (1997), Parker and Toniolo (2007) and Lamb et al. (2010) have all shown that at steady state, flows with hyperpycnal potential plunge at a densimetric Froude number of 1. However the analysis in these studies is mostly two dimensional and based on the idea of a depth limited plume. Tseng and Chou (2018) simulated hyperpycnal flows using a three dimensional analysis software and reported Froude number values from 0.64 to 1.72. Hence it is expected that negatively buoyant flows can plunge for densimetric Froude number values other than unity.

1.4 Study Approach

The research questions listed above are explored in this thesis using the hydrodynamic modeling package Delft3D. The next chapter provides an overview of Delft3D along with the details associated with the experimental matrix used to test the hypotheses. An expanded literature review on hyperpycnal flows can be found in Appendix A.

Chapter 2

Methods

2.1 Overview

The research questions discussed in Section 1.3 were tested by carrying out a series of simulations using Delft3D, a hydrodynamic modeling software developed by Deltares. Delft3D is a fully integrated software suite which facilitates three dimensional hydrodynamic and sediment transport simulations for river, estuarine, and coastal environments. It can carry out calculations in support of waves, water quality, and ecology studies. Two additional reasons that Delft3D was selected for this study are that, (1) it has been used to study the channelized discharges into open embayments (e.g., Edmonds et al., 2009; Caldwell and Edmonds, 2014; Jiménez-Robles et al., 2016; Robles and Sanchez, 2018); and, (2) the source code is freely available through Deltares. The source code for the software and the Graphical User Interface (GUI) was obtained from Deltares. The software was compiled on a 64-bit, 2.4 GHz Dell Precision T7810 using Microsoft Visual Studio 2017 and Intel FORTRAN Compiler 18.0.

The FLOW module of Delft3D allows for simulation of multi-dimensional hydrodynamic flows and transport phenomena. The numerical hydrodynamic modelling system Delft3D-FLOW solves the unsteady shallow water, or layer averaged, equations in 2D (single layer) or 3D (multilayer) (Deltares, 2018). The equations are based on the 3D Naiver-Stokes equations but are averaged over turbulent time scales and over a vertical layer. The system of equations consists of the horizontal equations of motion, the continuity equation, and the transport equations for conservative constituents (Deltares, 2018). A complete list of assumptions and approximations can be found in Deltares (2018). More details regarding Delft3D FLOW are discussed in 2.2.

2.2 Delft3D Introduction

2.2.1 Delft3D FLOW Assumptions

The Delft3D FLOW module solves 2D (depth averaged) or 3D non-linear shallow water equations, derived from the three dimensional Navier-Stokes equations for incompressible surface flows (Deltares, 2018). However, there are certain assumptions and approximations built in the software that are applied to any model simulated using the FLOW module. Some of the assumptions relevant to this study are listed below as given by Deltares (2018):

1. The σ coordinate system assumes depth to be much smaller than the horizontal length scale. Thus, vertical accelerations are assumed to be small compared to the gravitational acceleration.

2. The Boussinesq approximation holds true which means that the effect of variable density is only taken into account in the pressure term.

3. In the σ coordinate system, the immediate effect of buoyancy on the vertical flow is not considered. Vertical density differences are taken into account in the horizontal pressure gradients and in the turbulent exchange coefficients.

4. In a Cartesian frame of reference, the effect of Earth's curvature is not taken into account and the Coriolis parameter is assumed to be uniform unless specified otherwise.

5. The contribution of 3D turbulent eddies to the vertical exchange of horizontal momentum and mass is modelled by a vertical eddy viscosity and eddy diffusivity coefficient.

The coefficients can be specified or computed by means of an algebraic turbulence model [$(k-L)$ or $(k-\epsilon)$].

6. Without specification of a temperature model, the heat exchange through the free surface is zero. The heat loss through the bottom is always zero.

2.2.2 Governing Equations

Delft3D FLOW solves the Navier Stokes equations for an incompressible fluid, under the shallow water and the Boussinesq assumptions. The vertical accelerations are neglected in the vertical momentum equation which leads to the hydrostatic pressure equation. The vertical velocities are computed from the continuity equation. In the horizontal direction, Delft3D FLOW uses orthogonal curvilinear coordinates. Two coordinate systems are supported: Cartesian coordinates (ξ, η) and Spherical coordinates (λ, ϕ). The equations are formulated in orthogonal curvilinear coordinates. In the vertical direction, Delft3D FLOW offers two different vertical grid systems: the σ coordinate system $(\sigma - model)$ and the Cartesian Z coordinate system $(Z - model)$. By default, the hydrodynamic equations are valid for the σ coordinate system unless the $(Z - model)$ is specified.

The σ coordinate system

In this system, the vertical grid consists of layers which are bounded by two σ planes, which are not strictly horizontal but they follow the bottom topography and the free surface respectively. This gives a smooth representation of the topography. The number of layers over the entire horizontal computational area is constant, irrespective of the water depth (Figure 2.1). The σ coordinate system is defined as:

$$\sigma = \frac{z-\zeta}{d+\zeta} = \frac{z-\zeta}{H} \tag{2.1}$$

where z is the the vertical coordinate in space, ζ is the free surface elevation above the reference plane (at $z = 0$), d is the depth below the reference plane and H is the total water depth (Deltares, 2018). At the bottom, σ = -1 and at the free surface σ = 0. The layer of interfaces are chosen based on planes of constant σ, i.e the number of layers is the same at every location in the horizontal plane. For each layer, a set of coupled conservation equations are solved.

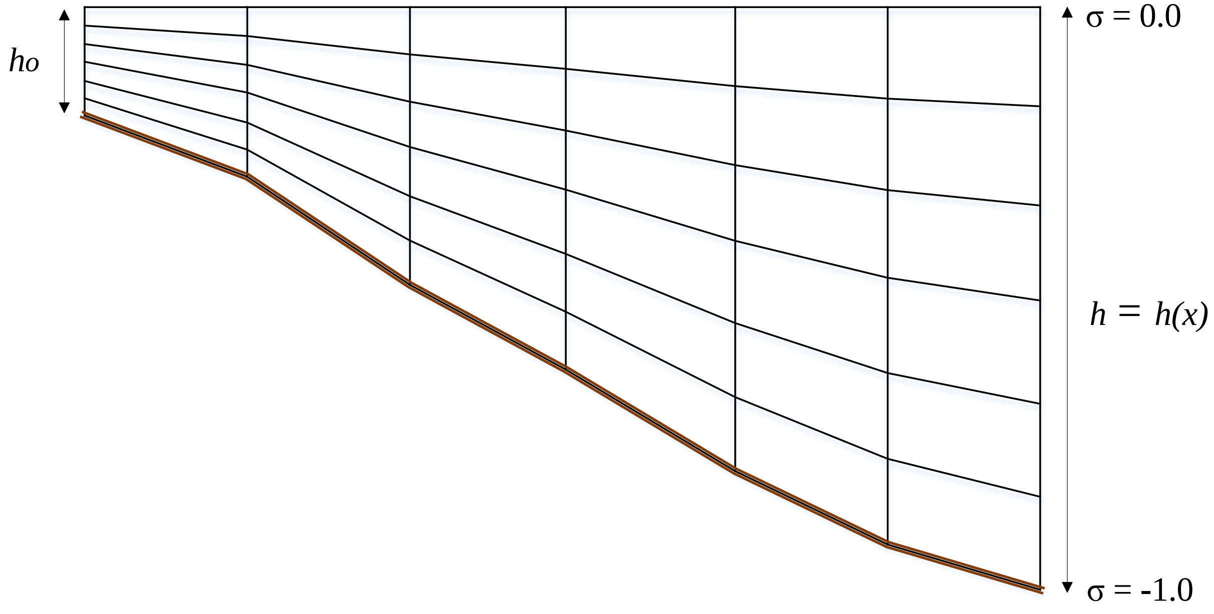

Figure 2.1: Example of a σ grid.

The continuity equation

The depth averaged continuity equation is derived by integrating the continuity equation for incompressible fluids ($\nabla \cdot \overrightarrow{u} = 0$) over the total depth. This integration takes into account the kinematic boundary conditions at water surface and bed level. The continuity equation is given by:

$$\frac{\partial \zeta}{\partial t} + \frac{1}{\sqrt{G_{\xi\xi}}\sqrt{G_{\eta\eta}}}\frac{\partial((d+\zeta)U\sqrt{G_{\eta\eta}})}{\partial \xi} + \frac{1}{\sqrt{G_{\xi\xi}}\sqrt{G_{\eta\eta}}}\frac{\partial((d+\zeta)V\sqrt{G_{\xi\xi}})}{\partial \eta} = (d+\zeta)Q \quad (2.2)$$

where $\sqrt{G_{\xi\xi}}$ and $\sqrt{G_{\eta\eta}}$ are coefficients used to transform curvilinear to rectangular coordinates, U and V are the depth averaged velocities,

$$U = \frac{1}{d+\zeta}\int_{d}^{\zeta} u dz = \int_{-1}^{0} u d\sigma \quad (2.3)$$

$$V = \frac{1}{d+\zeta}\int_{d}^{\zeta} v dz = \int_{-1}^{0} v d\sigma \quad (2.4)$$

and Q represents the contributions per unit area due to the discharge/withdrawal of water, precipitation and evaporation:

$$Q = \int_{-1}^{0}(q_{in} - q_{out})d\sigma + P - E \quad (2.5)$$

where q_{in} and q_{out} are the local sources and sinks of water per unit volume respectively, P is the non-local source term for precipitation and E the non local sink term due to evaporation.

Momentum equations in horizontal direction

The momentum equations in ξ- and η- direction are given by:

$$\frac{\partial u}{\partial t} + \frac{u}{\sqrt{G_{\xi\xi}}}\frac{\partial u}{\partial \xi} + \frac{v}{\sqrt{G_{\eta\eta}}}\frac{\partial u}{\partial \eta} + \frac{\omega}{d+\zeta}\frac{\partial u}{\partial \sigma} - \frac{v^2}{\sqrt{G_{\xi\xi}}\sqrt{G_{\eta\eta}}}\frac{\partial\sqrt{G_{\eta\eta}}}{\partial \xi} + \frac{uv}{\sqrt{G_{\xi\xi}}\sqrt{G_{\eta\eta}}}\frac{\partial\sqrt{G_{\xi\xi}}}{\partial \eta}$$
$$-fv = -\frac{1}{\rho_0\sqrt{G_{\xi\xi}}}P_{\xi} + F_{\xi}\frac{1}{(d+\zeta)^2}\frac{\partial}{\partial \sigma}(\nu_v\frac{\partial u}{\partial \sigma}) + M_{\xi} \quad (2.6)$$

$$\frac{\partial v}{\partial t}+\frac{u}{\sqrt{G_{\xi\xi}}}\frac{\partial v}{\partial \xi}+\frac{v}{\sqrt{G_{\eta\eta}}}\frac{\partial v}{\partial \eta}+\frac{\omega}{d+\zeta}\frac{\partial v}{\partial \sigma}+\frac{uv}{\sqrt{G_{\xi\xi}}\sqrt{G_{\eta\eta}}}\frac{\partial\sqrt{G_{\eta\eta}}}{\partial \xi}-\frac{u^2}{\sqrt{G_{\xi\xi}}\sqrt{G_{\eta\eta}}}\frac{\partial\sqrt{G_{\xi\xi}}}{\partial \eta}$$
$$-fu=-\frac{1}{\rho_0\sqrt{G_{\eta\eta}}}P_\eta+F_\eta\frac{1}{(d+\zeta)^2}\frac{\partial}{\partial\sigma}(\nu_v\frac{\partial v}{\partial \sigma})+M_\eta \tag{2.7}$$

Forces F_ξ and F_η in the momentum equations represent the unbalance of horizontal Reynold's stresses. M_ξ and M_η represent the contributions due to external sources or sinks of momentum and f represents the Coriolis parameter (inertial frequency).

For the σ grid, under the shallow water assumption, the vertical momentum equation is reduced to a hydrostatic pressure equation. Vertical accelerations due to buoyancy effects and due to sudden variations in the bottom topography are not taken into account (Deltares, 2018). Other important mathematical formulations of the 3D shallow water flow and transport model and information regarding the numerical solutions methods applied in Delft3D FLOW can be found in detail in chapters 9 and 10 of Deltares (2018). The description provided here applies in most cases for the vertical σ coordinate system.

2.3 Model Setup and Simulations

2.3.1 Overview

In order to answer the research questions that concern with the lateral spreading of the plume, simulations were performed on two hypothetical domains in Delft3D: (i) A channel flowing into an unbounded domain which is analogous to a river flowing into an open embayment and (ii) A channel laterally confined on both sides throughout its length. The purpose of analyzing the plunge phenomenon in a laterally confined channel is to study the traditional

2D plunging, with it's depth limiting criteria and to highlight the differences that occur as a result of lateral expansion of the plume in an unbounded basin. The domain characteristics in the unbounded case have been discussed in Section 2.3.2. The laterally confined case uses the same domain characteristics, with the exception that the channel is surrounded by land boundaries on both sides throughout its length to maintain confined flow.

2.3.2 Domain Characteristics

The analysis was performed on a hypothetical domain of a river entering a large basin of water without waves, tides, base-level changes, or sediment (Figure 2.2). The domain is 7025 meters long in both cross-shore and the along-shore direction with the river placed at the center in the along-shore direction. The model is computed on a uniform 25 m x 25 m grid. The bathymetry of the domain varies according to the simulations and depends on the basin floor slope which ranges from 0 m/m to 0.1 m/m. At the western boundary, a channel that is 225 meters wide, 3 meters deep, and 1000 meters long is carved into a land boundary (beach). The beach elevation is high enough that the water is confined to the river throughout all simulations. Open boundaries of constant water surface elevation are placed along the north, east and south boundaries of the grid and that of incoming water discharge (Q = 1000 cms) at the channel on the western boundary. The domain is split into 15 equal layers in the vertical direction using the σ coordinate system (σ model) in the z direction. A detailed explanation of the σ coordinate system is given in Section 2.2.2. Each simulation is run for 12 hours, which allows for plunge formation to reach steady state.

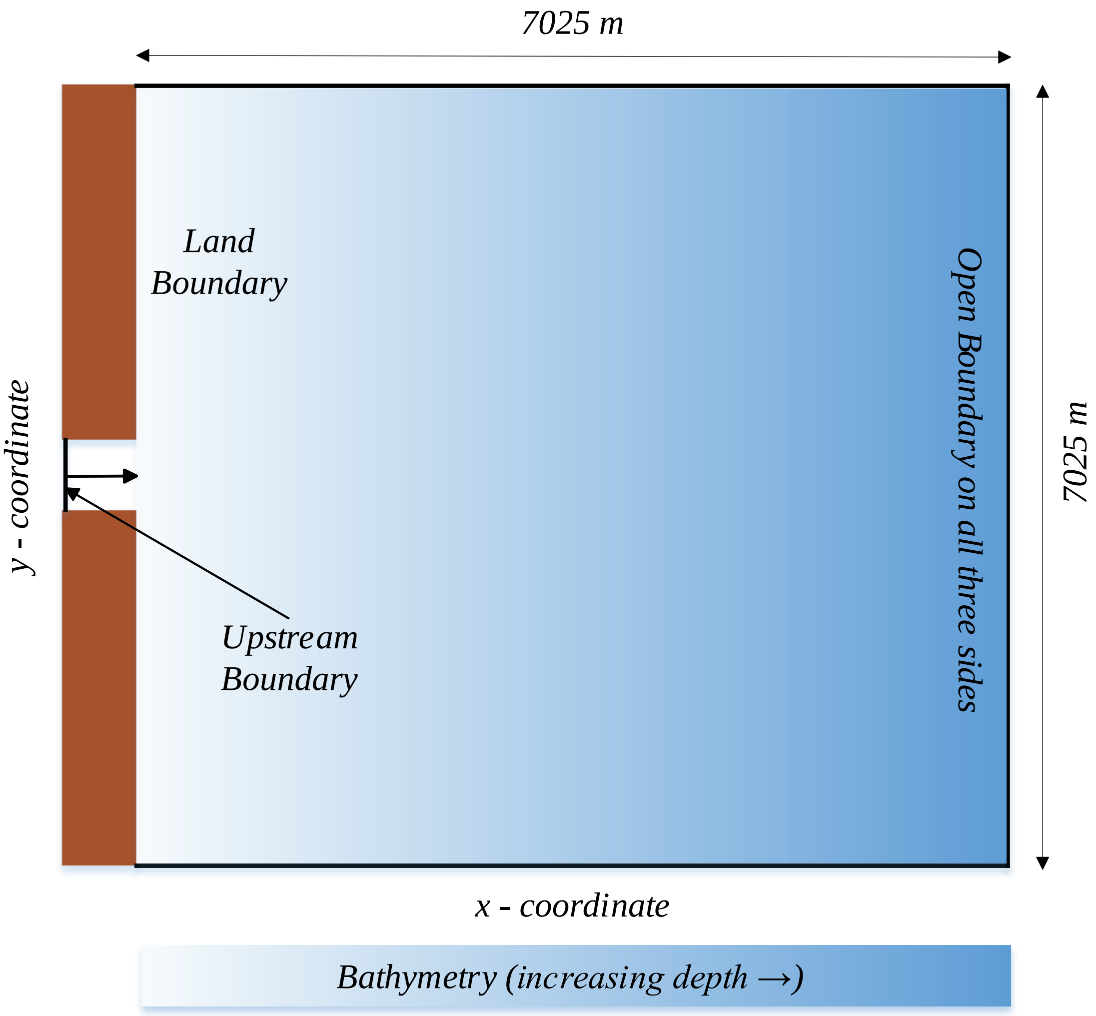

Figure 2.2: Model setup for the domain (plan view)

2.3.3 Simulation Details

The model uses salinity to drive the density difference between the inflow and the ambient basin. Three different scenarios have been simulated (listed in Table 2.1), that induce three different density differences to test out the hypotheses. For every scenario, the parameters of basin slope (S) and the bottom roughness (Chézy friction coefficient, C_z) have been varied as shown in table 2.2. The three scenarios (density differences), six basin slopes and three Chézy coefficients resulted in a total of 54 model runs.

Scenario	Salinity (ppt)		Density difference
Number	Inflow	Ambient	kgm^{-3}
1	55	31	18
2	24	0	18
3	12	0	10

Table 2.1: Flow Simulation Scenarios

Parameter	Values
Slope (m/m)	0, 0.001, 0.003, 0.005, 0.01, 0.1
Chézy friction coefficient	45, 55, 65

Table 2.2: Parameter values

2.3.4 Model Parameters

All user defined model parameters, common for all experimental runs are listed in table 2.3. The reference level for our model is specified at 0 meters. Domain bathymetry, initial water level and boundary water levels are all defined with respect to this reference level. For all our experimental runs, we specify the channel depth to be -5 meters, i.e. 5 meters below the reference level and the water level (both initial and at sea boundary) to be -2 meters, giving a flow depth of 3 meters within the channel. We specify negative values for the Thatcher-Harleman time lags in order to fully exclude the influence of outer world on the inner model domain. Thus, the solution for salinity, which in turn affects the density, will be fully determined by the processes inside the model area (Deltares, 2018). To model the 3D turbulence, a $k-\epsilon$, second order turbulence closure formulation is used to determine the vertical turbulent eddy viscosity and eddy diffusivity coefficients by transport equations for turbulent kinetic energy and its dissipation. The "correction for sigma coordinates" option available in Delft3D FLOW, that minimizes artificial vertical diffusion and truncation errors, has been applied to all the simulations. This implements a method which gives a consistent, stable and monotonic approximation of both the horizontal pressure gradient and the horizontal diffusion term (Deltares, 2018). Two additional parameters have been implemented by adding flags (keywords) in the model. First, the baroclinic pressure is switched off for all open boundaries. This is done to exclude the influence of the concentration boundary conditions on the flow inside our domain due to the baroclinic pressure term. Secondly, the advection terms at the offshore boundary, that may generate an artificial boundary layer along the boundary, have been switched off (Deltares, 2018).

User Defined Model Parameter	Value	Units
Grid size	281x281	cells
Cell size	25x25	m
Number of layers in vertical	15	-
Inflow Channel dimensions	225x3	m
Time step	0.1	min
Upstream open boundary: incoming water discharge	1000	m^3s^{-1}
Downstream open boundaries: constant water surface elevation	-2	m
Thatcher-Harlemann time lags	-1	-
Gravity	9.81	ms^{-2}
Horizontal eddy viscosity	1	m^2s
Horizontal eddy diffusivity	10	m^2s
Model for 3D turbulence	k-ϵ	-

Table 2.3: Parameter values

2.4 Analysis Methods

This section discusses the theoretical framework used to interpret the results from Delft3D simulation outputs. A primary component of this section is to provide an understanding of the plunge point and define the terms of incipient plunge point, plunge point and the plume width that have been used in the analysis. This is intended to give a more robust comprehension of the results and discussion of the research.

2.4.1 Incipient Plunge Point

The concept of an incipient plunge point was first put forth by Lee and Yu (1997). The idea behind incipient plunging is that as dense inflow from the river (plume) enters a basin with an ambient water density, the plume travels some distance into the basin before mixing starts affecting the plume density. So an incipient plunge point would be the first location in the direction of flow (x_i) where a significant difference in density $(\rho_{x_i} - \rho_{x_{i-1}}) > K$ is observed as we move along x. For this study, the incipient plunge point was located by observing the channel centerline density values in the topmost layer along the x-direction with $K = 0.1\ kgm^3s^{-1}$. This is the location where the density of plume starts decreasing rapidly as it progresses in the domain. The incipient plunge point location is illustrated for one simulation with the help of Figure 2.3 for a better understanding.

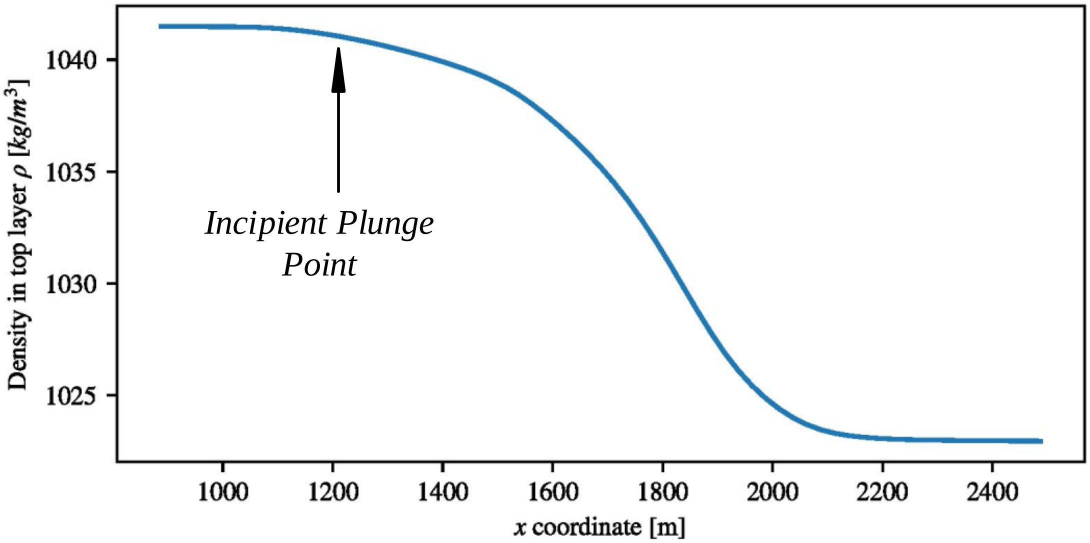

Figure 2.3: Location of the incipient plunge point for simulation 10 based on centerline density in the top layer

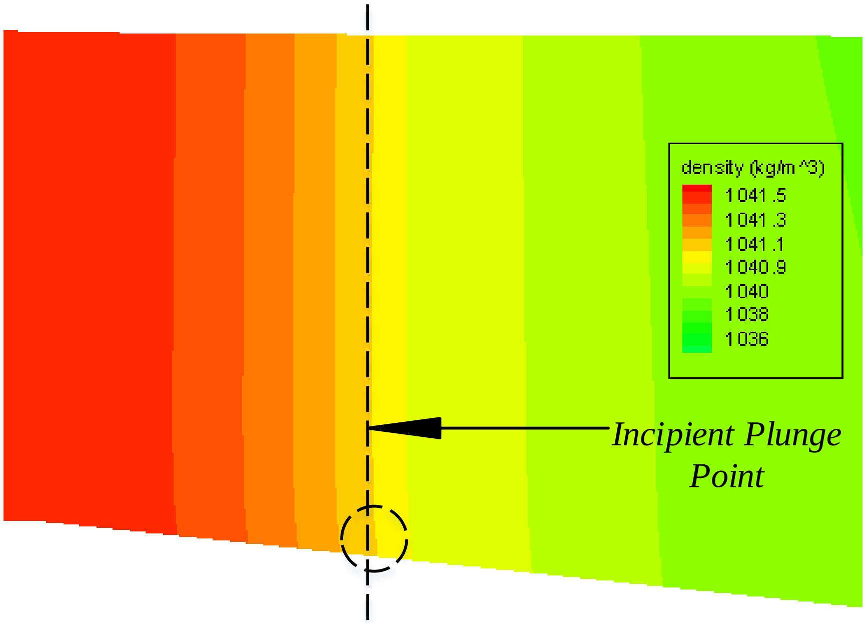

Figure 2.4: Density contours explaining the incipient plunge location where the density in top layer decreases, and a small bulge in the contour appears at the bottom,

2.4.2 Plunge Point

Density of the flow in the top layer starts decreasing rapidly than that in the bottom layer. This can be understood with the help of density contours shown in Figure 2.5. It can be seen from the figure that while density is reduced in the top layer, at the same location, the bottom layer is propagating with a higher density. Hence to determine plunge location of the plume as a whole, density across the entire depth needs to be considered. For this reason we make use of the depth averaged density in the calculation leading to the determination of the plume plunge point.

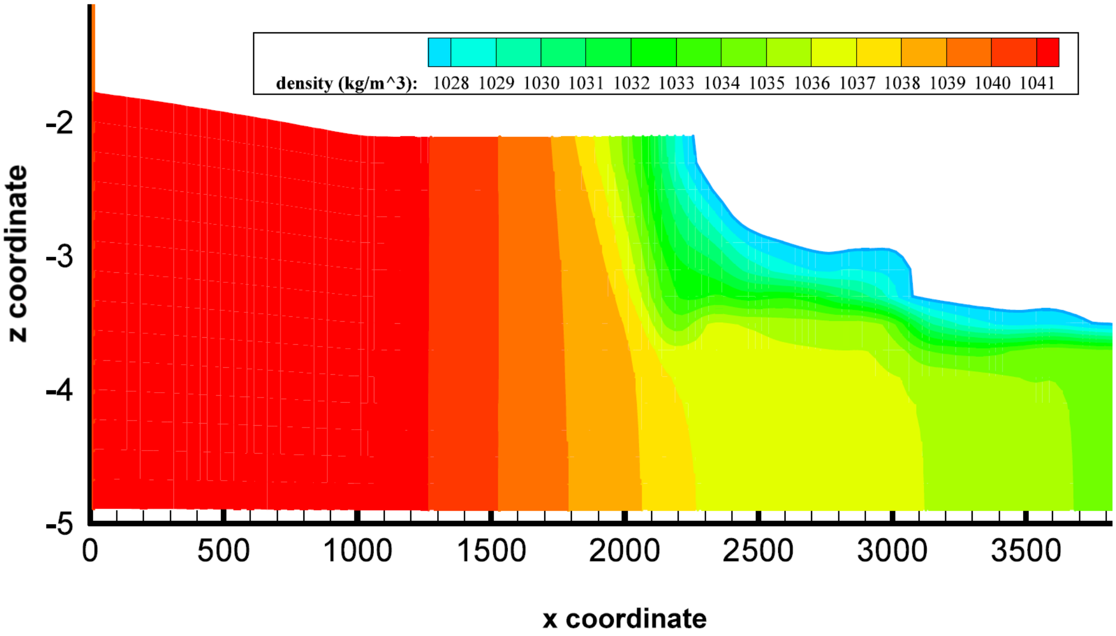

Figure 2.5: Density contours along centerline for simulation 1.

In this study, the location of plunge point is established based on densimetric Froude number given by equation 1.1. The variation of the densimetric Froude number along centerline, as the plume travels in the flow direction, is shown in Figure 2.6. The values of flow depth (h), depth average velocity (U) and density (ρ) for the calculation of Fr_d are available from the Delft3D run output. The figure illustrates that as the flow exits the river, the densimetric Froude number starts declining as the velocity decreases and the flow depth increases with the bathymetry. This trend continues until a point after which, the density difference ($\Delta\rho$) starts decreasing significantly and has the dominant effect in the Froude number calculation. As a result, after this point the densimetric Froude number increases in a short period where the plume density approaches ambient water density. We define the plunge location of the plume as this point where the Fr_d reaches a minimum before increasing again. This can be understood with the help of Figure 2.7. At the plunge point, the bottom layer begins to show a bulge in the density contours indicating that dense flow begins to sink to the bottom. Figure 2.8 shows the plan view of the top layer and the centerline cross sectional view of density values for simulation 10, indicating incipient and the actual plunge point.

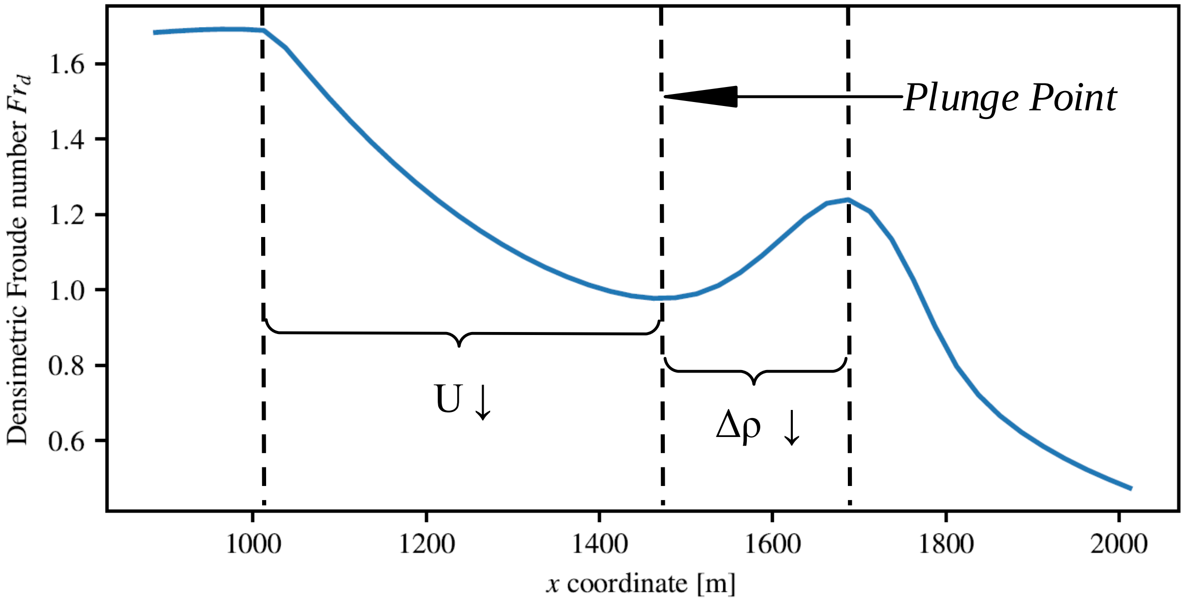

Figure 2.6: Densimetric Froude number at channel centerline for simulation 19

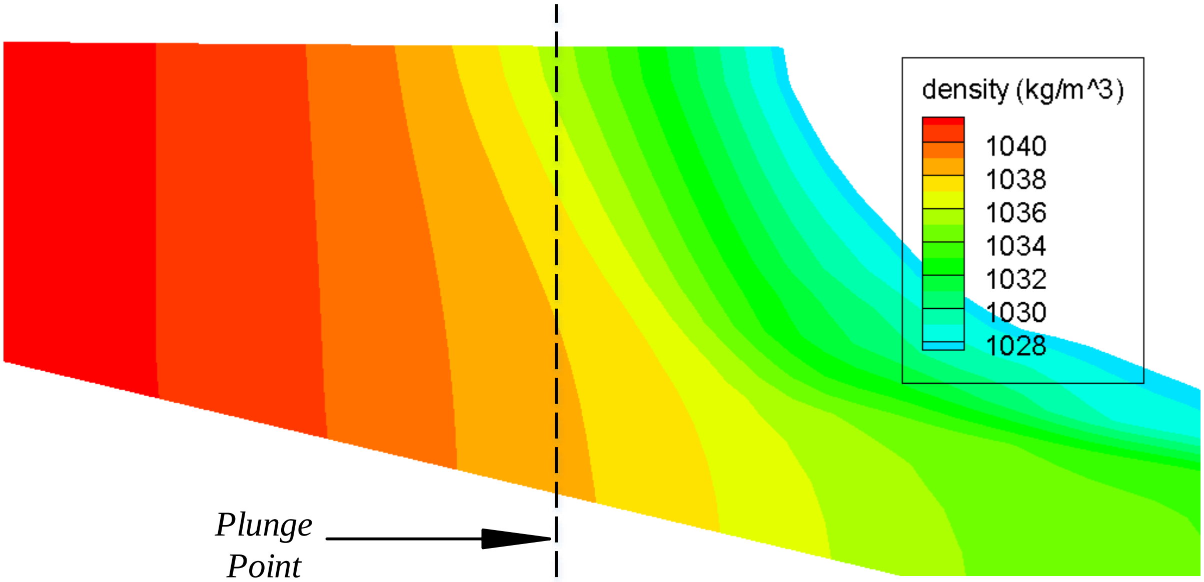

Figure 2.7: Density contours at centerline profile explaining the plunge point for simulation 19.

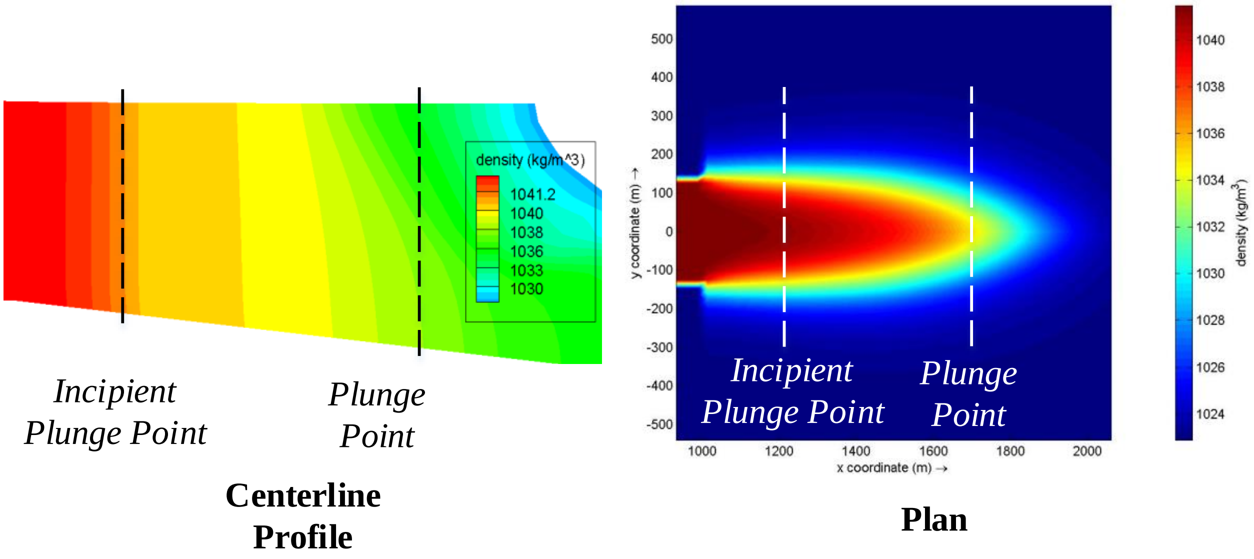

Figure 2.8: Profile and Plan views of density contours with incipient and actual plunge points for simulation 10.

2.4.3 Plume Width

Another parameter that had to be calculated from the Delft3D output was the width of the plume up to the point of plunging. Previous studies involving plume width, mostly in the hypopycnal case, have all followed different approaches for the definition of the width. In this study, with the data available from Delft3D, we used the velocity component parallel to the flow direction (x-direction) u_x to define plume width. When the plume enters the domain after leaving the channel, the x-component of velocity u_x is a maximum at the centerline and decreases to zero on both sides in the alongshore direction. This is illustrated in Figure 2.9. In this study, the plume width is defined at any point in x, as the distance between the points in the y direction where velocity reaches 0.05 times the maximum centerline velocity. This makes sure that the area in the receiving basin beyond the plume is excluded and isn't considered in the calculation of plume width.

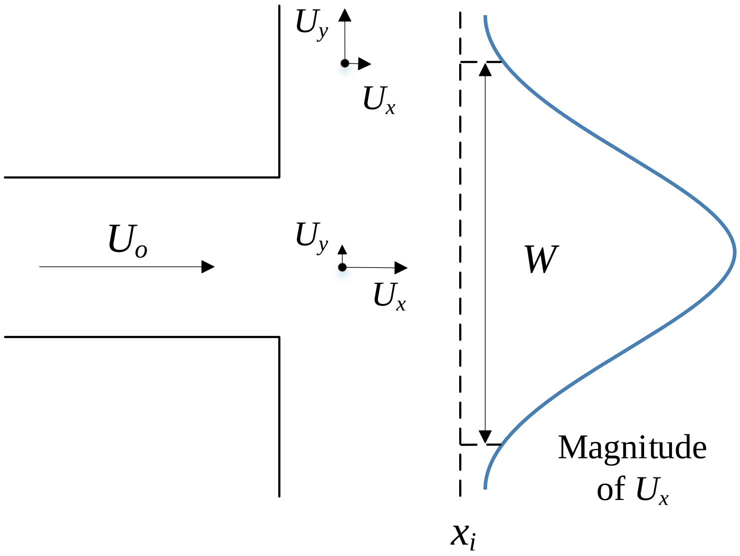

Figure 2.9: Definition of the velocity components and plume width.

2.4.4 The Jet Model and 2D channel analysis

The theoretical plunge point is associated with a standard 2D analysis (Equation 1.4) and a layer-averaged jet model approach (Strom and Bhattacharya, 2012). All calculations were done using the boundary conditions from the Delft3D simulations. These additional theoretical plunge points were calculated to better highlight the effects that the laterally unbounded basin has on plunging. The jet model accounts for lateral entrainment of ambient fluid as the river discharge expands into an unbounded domain.

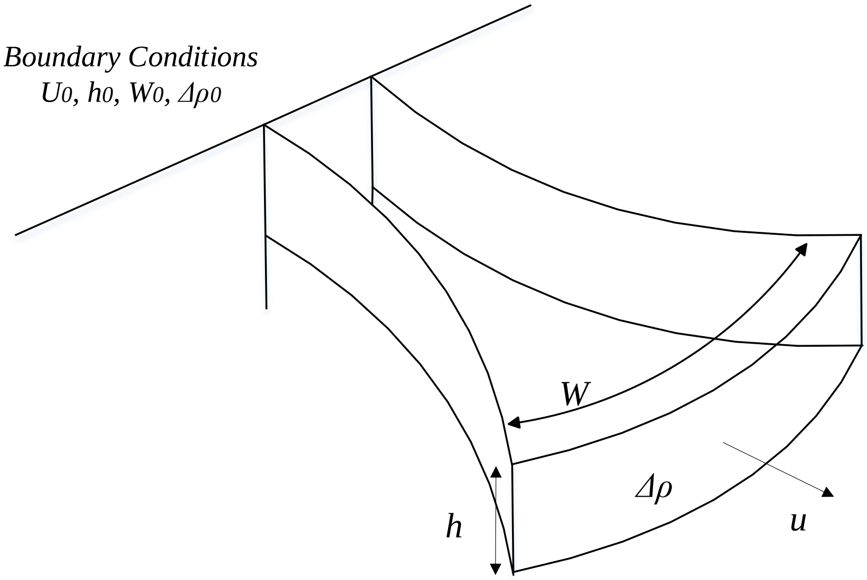

Figure 2.10: Setup of the layer-averaged jet model.

Entrainment impacts the longitudinal development of the densimetric Froude number by decreasing velocity and decreasing the fluid density of river discharge. The analysis is carried out by solving steady-state jet equations for a river discharging with the application of the Boussinesq approximation. The key variables in developing the equation are the volume flow rate $Q = WhU$, momentum $M = QU$, buoyancy flux $B = g'Q$ where $g' = g(\rho - \rho_a)/\rho_a$

is the reduced gravity. The model is developed by solving conservation equations of volume, mass and momentum given by:

$$\frac{dQ}{dx} = E \tag{2.8}$$

$$\frac{dM}{dx} = -F_\tau \tag{2.9}$$

$$\frac{dB}{dx} = 0 \tag{2.10}$$

where E is the entrainment rate per unit length and F_τ is boundary friction per unit length. Top-hat profiles are assumed for all integral quantities and flow is assumed to be attached to the bed over the region of interest. The closure equations for the model are

$$E = 2\alpha h U \tag{2.11}$$

$$F_\tau = C_f W U^2 \tag{2.12}$$

where α is the lateral entrainment coefficient and C_f is the friction coefficient. The model of equations is solved using 4th-order Runge-Kutta along with the closure equations, inlet boundary conditions $[W_0, h_0, U_0, \rho_0]$, basin conditions [ρ_a, slope $= \theta$] and values for α and C_f.

In case of the 2D channel analysis, the governing equation becomes

$$\frac{dQ}{dx} = 0 \tag{2.13}$$

with the same definitions of Q, h, W and ρ as above.

The plunge points calculated by all the three methods viz. Delft3D, the Jet Model and the 2D channel analysis are given in chapter 4.

Chapter 3

Model Development and Validation

During the development of a simulation model, the ultimate goal is to build a model that is credible and gives accurate results. This goal is recognized by the verification and validation of computer simulation models. Any modeling study obtains results by analyzing the data obtained from the model. It is for this reason that the model developers and users are concerned with its "correctness". Verification and validation of the simulation model address this concern. This process is usually carried out after all the functional specifications have been provided and the initial model has been developed.

In this study, the main concern was whether Delft3D is able to accurately simulate the flow processes and interactions of a river inflow into an unconfined domain. To validate our model and justify the use of Delft3D, simulations were also carried out to compare the Delft3D output with results from two studies: Jiménez-Robles et al. (2016) and Tseng and Chou (2018). The main objective was to check that the flow behaviour and patterns observed closely resemble the expected outcomes. The Delft3D models built for these validation studies had the exact same physical conditions and model parameters as that in the original studies.

Jiménez-Robles et al. (2016) computed plane jet hydrodynamics and morphodynamics of a river mouth bar in fluvially dominated deltas. They used a simplified, one layer domain that represented the shoreline and a river flowing into the continental shelf, similar to this study. Open boundaries of constant water surface elevation were specified at the sea and a constant river discharge flux boundary was prescribed on the landward boundary. It is previously known that jet hydrodynamics are characterized by centerline velocity and lateral expansion. To test whether jet hydrodynamics follows self-similarity conditions, Jiménez-Robles et al. (2016) normalized the mean longitudinal velocity component by the jet center velocity (U/U_c) and reported the values along a transverse transect located at $x = 500$ meters from the river outlet. The velocity distribution results from Jiménez-Robles et al. (2016) are compared with those from the validation study in Figure 3.1. The y coordinate is normalized similar to that in Jiménez-Robles et al. (2016), with respect to the jet half width $b(x)$. The figure illustrates that the velocity distribution results from Delft3D follow a near-Gaussian shape, similar to the results from Jiménez-Robles et al. (2016) which indicates self-similarity of the jet with respect to the centerline.

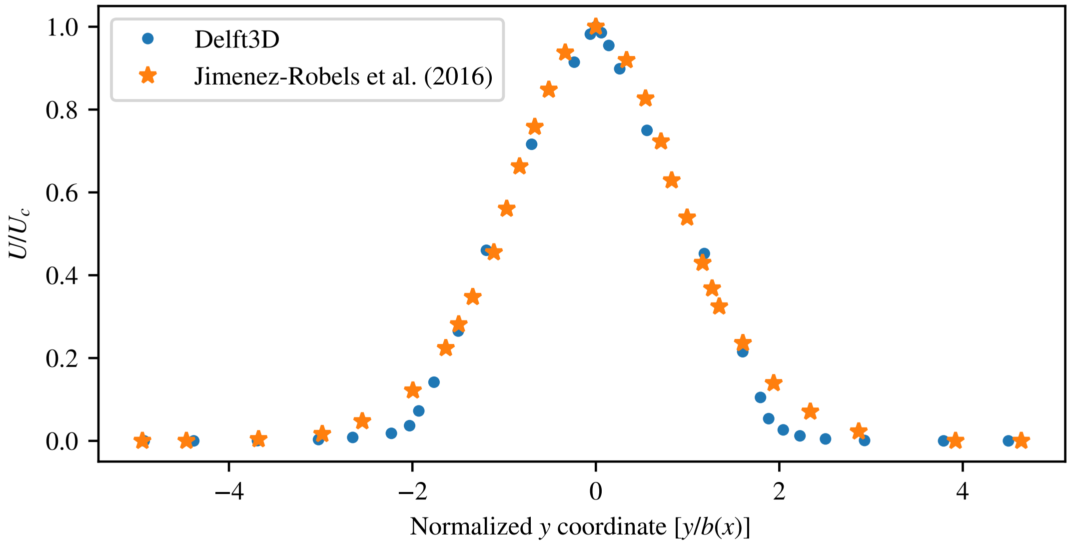

Figure 3.1: Comparison of normalized velocity distribution of the mean longitudinal velocity U/U_c along a cross section located at $x = 500$ meters from river mouth

Jiménez-Robles et al. (2016) also observed that in their simulations, the centerline velocity starts to decay as soon as the jet leaves the channel. They verified the effects of bottom slope on jet stability by visually inspecting depth-averaged velocity fields for both horizontal and sloping bottoms. They stated that the jet remains unaltered for horizontal slopes but for higher slopes, it becomes unstable leading to the appearance of a distorted velocity field. The depth-averaged velocity fields for both cases and its counterparts for our Delft3D validation model are shown in Figure 3.2. The validation model predicts similar velocity fields for both bottom slope conditions.

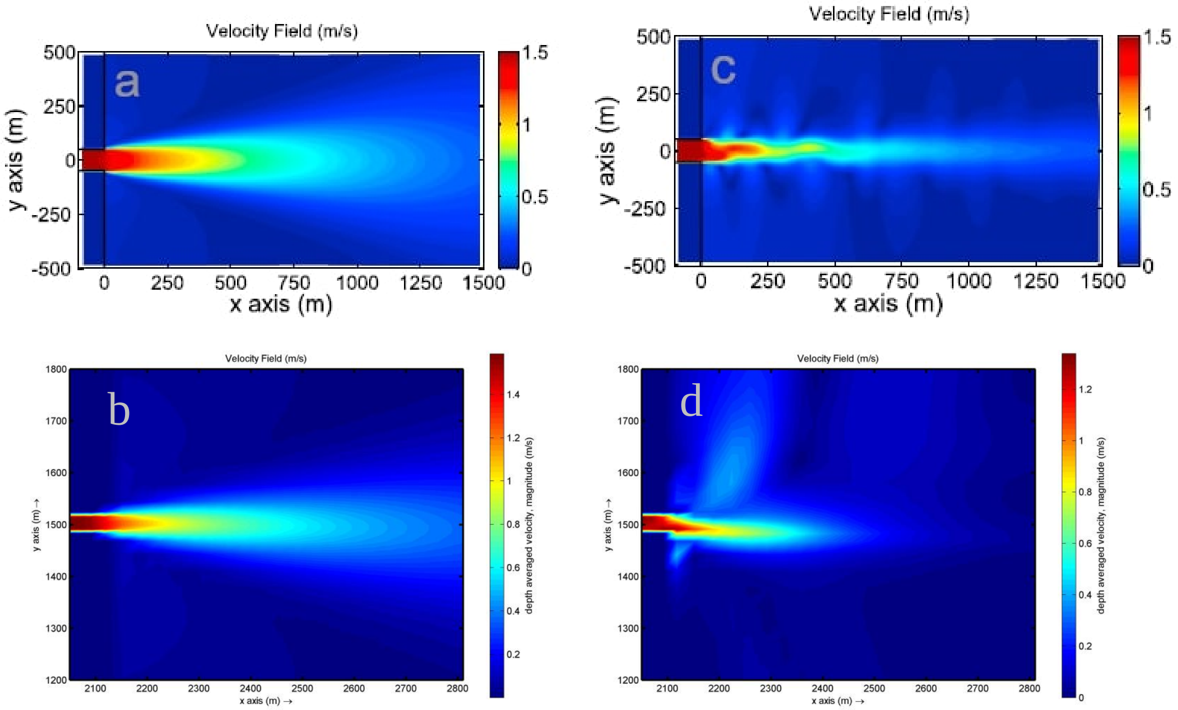

Figure 3.2: Comparison of velocity fields computed with Delft3D (panels c and d) with a horizontal and sloping bottom for Jiménez-Robles et al. (2016) (panels a and b).

Tseng and Chou (2018) simulated an idealized domain of a straight river channel flowing into an open ocean similar to that in Chen et al. (2013), using a 3D hydrodynamics model SUNTANS. Two slopes of 0.005 (medium) and 0.01 (steep) were used in their study. A suspended sediment concentration (SSC) of 50 g/l was specified as the inflow boundary condition and that of 0 g/l was specified at open boundary conditions in the ocean. Velocity of the incoming river flow was taken as 2 m/s. A similar model was built using Delft3D to conduct a validation study. The main aim of this validation study was to check whether the plume dynamics and structure simulated using Delft3D was similar to that from Tseng and Chou (2018). The validation study used salinity to induce density difference in the domain which serves a similar function as that of the SSC. Tseng and Chou (2018) presented a visualization of the plume structure by reporting a series of snippets of SSC contours in the vertical transect at the centerline (y=0) at different time steps through the simulation (Figure 3.3). This gives an idea regarding the development of the plume as the simulation progresses.

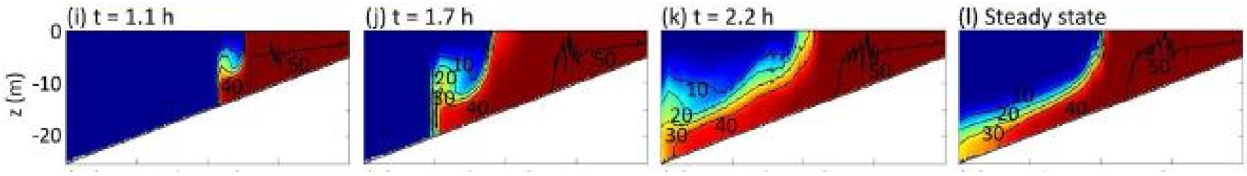

Figure 3.3: SSC contours at the vertical transect along the centerline as given in Tseng and Chou (2018)

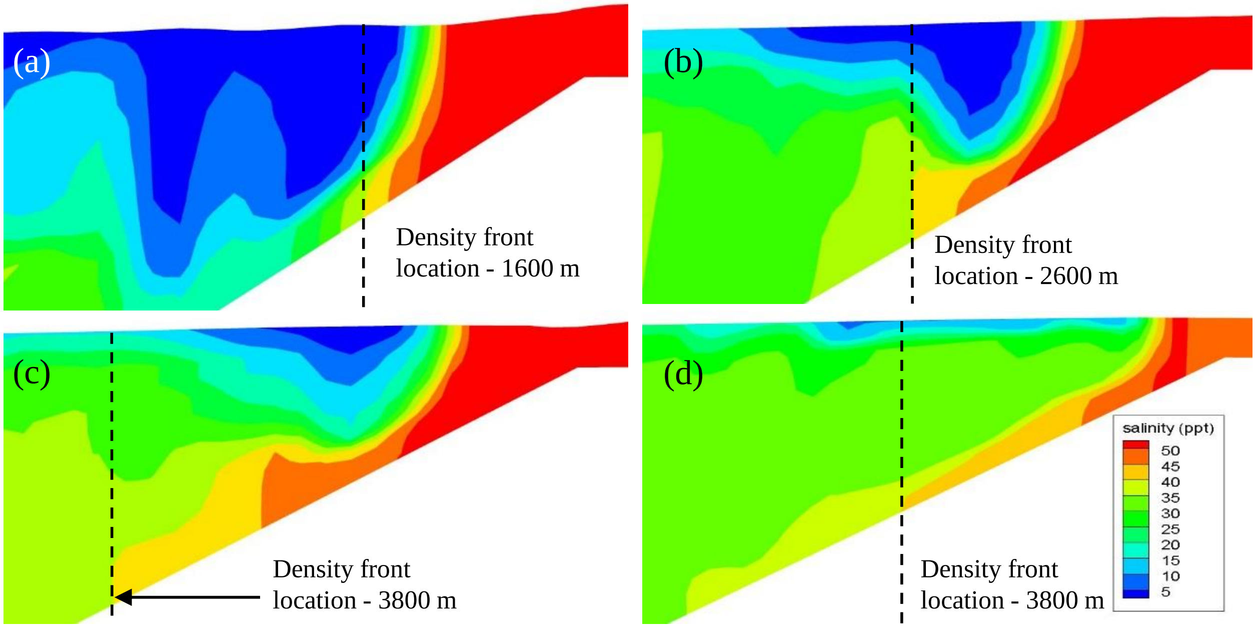

Figure 3.4: Snapshots (a-d) of salinity at the vertical transect along the centerline as predicted by Delft3D for times 3.5h, 4.5h, 5.5h and steady state respectively.

Figure 3.4 (a-d) shows snippets of salinity contours in the vertical transect at the centerline (y=0) from the Delft3D model at different time steps through the simulation. It can be seen that the plume development and its structure is similar to that produced by SUNTANS. The model by Tseng and Chou (2018) noted two important observations: (1) the plume begins to spread as it enters the continental slope, and (2) the spreading of plume is weaker at a steeper slope, i.e. the SSC concentrated more at the centerline. Delft3D model also produced similar results for cases with medium and steep slopes. This can be seen from Figure 3.5. The Delft3D model was also successful in predicting plunging closer to the river mouth at higher slopes as shown by Tseng and Chou (2018) in their study.

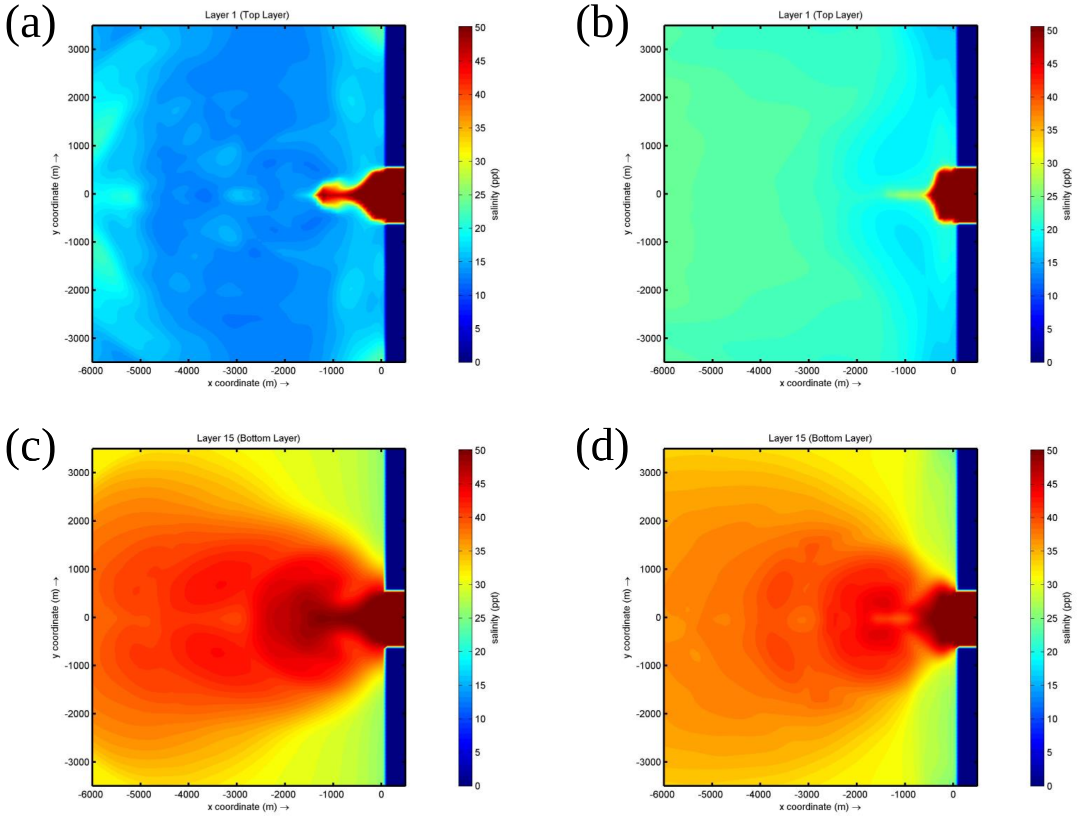

Figure 3.5: Plan views of salinity in the top layer (a,b) and the bottom layer (c,d) for medium (a,c) and steep (b,d) slopes. Figures a and b indicate plunging closer to the channel with increase in slope.Spreading of the plume can be seen from figures b and d.

Another important check was comparing the plunge location predicted by the validation model (Delft3D) to that given by SUNTANS in Tseng and Chou (2018). As mentioned above, Tseng and Chou (2018) reported plunge locations for medium and steep slopes. The plunge locations predicted by Delft3D are similar to that from Tseng and Chou (2018) as can be seen from table 3.1 and are shown in Figure 3.6.

Slope	Tseng and Chou (2018)	Delft3D
Medium	1628 m	1604 m
Steep	1036 m	1055 m

Table 3.1: Comparison of plunge location (x_p) predicted by Delft3D with the values reported by Tseng and Chou (2018)

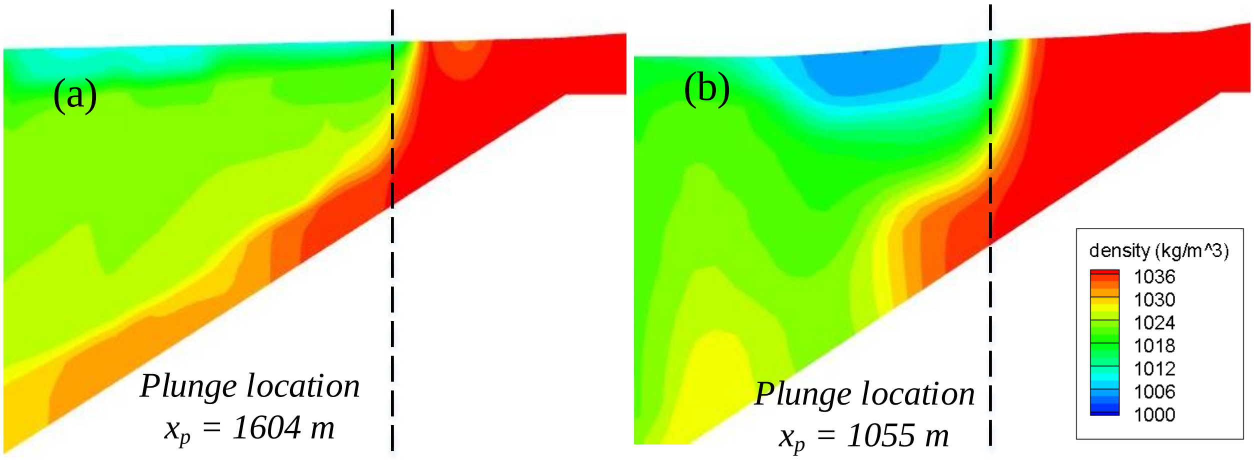

Figure 3.6: Plunge location predicted by Delft3D for medium (a) and steep (b) slopes given in Tseng and Chou (2018)

The three dimensional structure of the plume can also be seen with the help of iso-surfaces (Tseng and Chou, 2018). To get a clear understanding of the 3D plume structure during a steady state, an iso-surface of salinity 35 ppt, over the continental slope is shown in Figure 3.7.

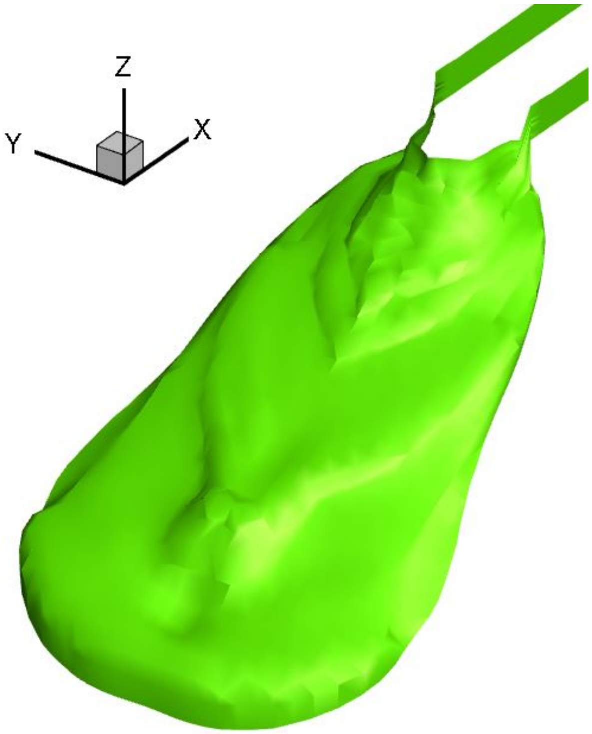

Figure 3.7: The iso-surface of salinity 35 ppt during steady state.

From the validation studies mentioned above, it can be seen that the models built using Delft3D are able to simulate the plunge phenomenon from a channel flowing into an unconfined domain and that Delft3D is able to capture details of the flow structure and velocity in the domain. Following validation studies, a grid independence study was conducted to finalize the mesh size to be used for simulations in this study.

Grid Independence

Grid independence is an important issue in any numerical modeling simulation. In a study involving a three dimensional spatial domain, deciding the grid size and dimensions is of prime importance. Ideally, a grid independent model is the one in which the solution is not affected by the size of the grid. To establish the grid independence, the model in this study was tested with grid sizes ranging from 212 meters to 20 meters. Figure 3.8 shows plan views for the top and bottom layers of density for simulations with grid sizes 212 m, 78 m, 30 m and 20 m respectively. No significant difference in the plume structure was observed between the 50 m, 30 m and the 20 m grids. Also, studies have been conducted by Edmonds et al. (2009), Caldwell and Edmonds (2014) and Robles and Sanchez (2018), that used Delft3D to model a domain of a river entering an unconfined domain of size similar to that adopted in this study. These studies also serve as a reference for the grid size. Initial grid independence tests and references helped finalize the size of the grid as 25 meters. This grid size also proved to be less expensive computationally.

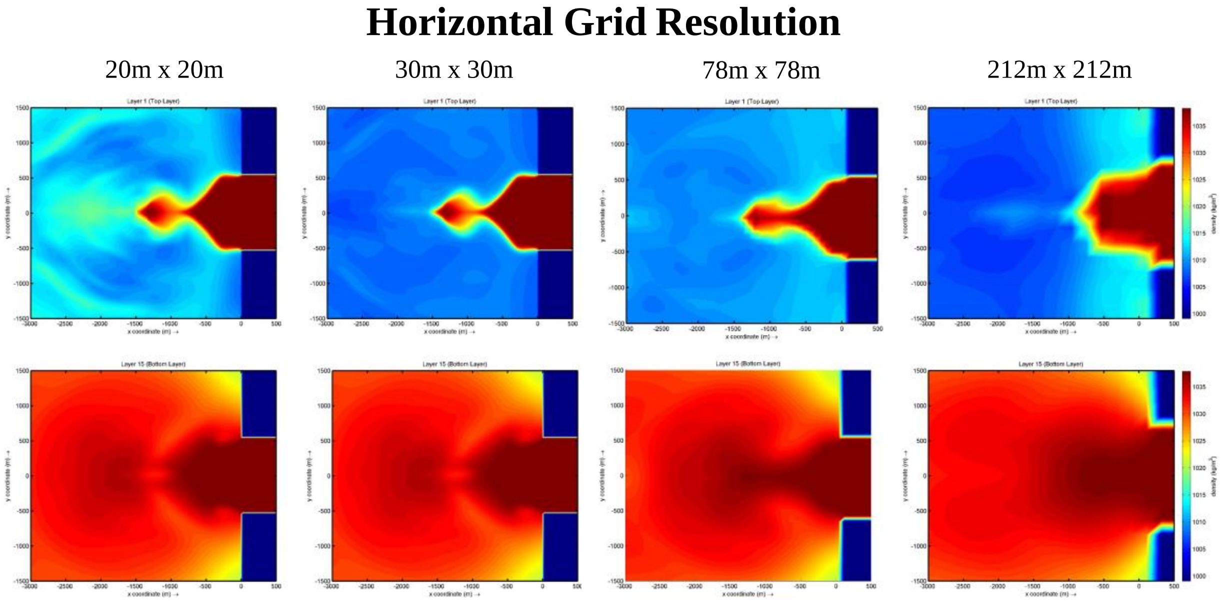

Figure 3.8: Comparison of plume structure (top view) in the bottom layer and the top layer for different grid resolutions

Check on plume width

The definition of plume width adopted in this study is given in Section 2.4.3. To verify the accuracy of this definition and the Delft3D model, a simulation was carried out for the hypopycnal case. The domain and the model parameters used were the same as those described in chapter 2, but with $\rho_0 < \rho_a$. This step served as a check on the model and the definition of width. Figure 3.9 shows a plot of the change in plume width (dW/dx) with respect to $\sqrt{R_i}$. Hetland (2010) developed a layer-averaged model for hypopycnal plumes which is described in appendix A.4. For comparison, the change in plume width as predicted by the layer model is also plotted on Figure 3.9. It is clearly seen that the dW/dx results for the adopted width definition are similar to those predicted by the layer model for the hypopycnal case. Thus, it can be said that Delft3D is capable of simulating river-fed plumes.

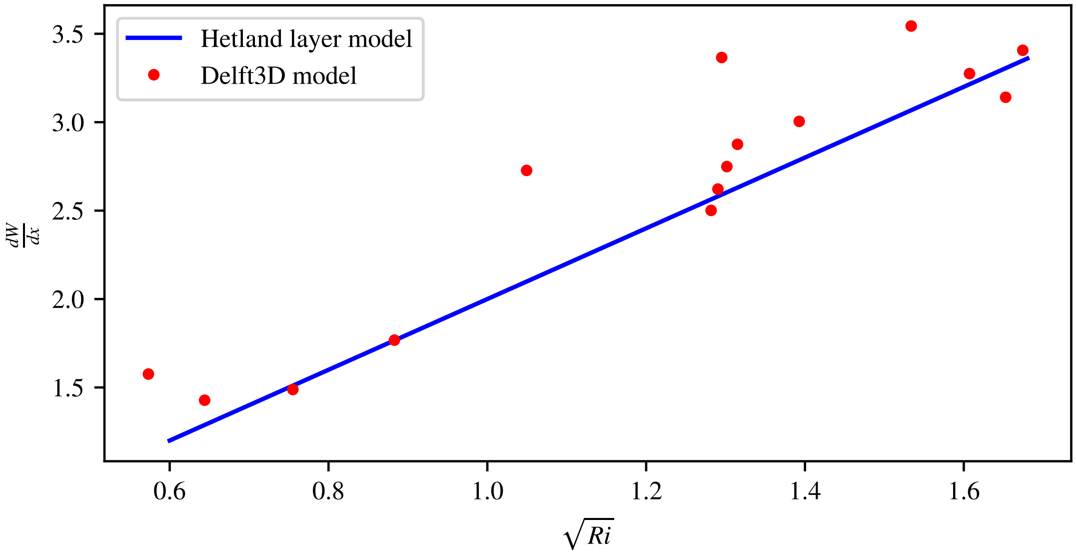

Figure 3.9: Verification of the Hetland (2010) layer model

These model validations serve an important purpose of checking the accuracy of model's representation of the real system. This chapter shows the capabilities of Delft3D in simulating river-fed plumes, both hypopycnal and hyperpycnal.

Chapter 4

Results

Results of the experimental simulations show the variation in estimated parameters of the location of plunge point, the densimetric Froude number, Fr_d, at the plunge point, and the plume width, $W = W(x)$, under varying bottom slopes, friction coefficients and density differences. The data required for density, velocity and flow depth for all simulations was extracted from QUICKPLOT, a built-in visualization and animation program associated with Delft3D. QUICKPLOT allows the user to view results in a plan view for the domain and also enables the user to quickly navigate across different time steps. This is extremely beneficial to ascertain the time when the plume reached a steady state and does not migrate further with time. For all experimental runs, the analysis was performed at time of 8 hours into the simulation, well into the steady state condition. The incipient plunge point, plunge point, and the densimetric Froude number at plunging (Equation 1.1) were all calculated with Python scripts that were run in Google's Colaboratory.

4.1 2D Plunging Overview

The plunge phenomenon in a laterally confined channel can be visualized with the help of Figure 4.1, which shows a density iso-surface for $\rho = 1040$. The figure illustrates that in case of a confined channel, the dense inflow plunges in the vertical z direction and advances forward in the x direction. The transition in density values can be seen with the help of Figure 4.2 that shows density contours along the x direction at a slice along the centerline.

This helps in understanding the difference between plunging in a confined basin and that in an unconfined basin which is discussed in the next section.

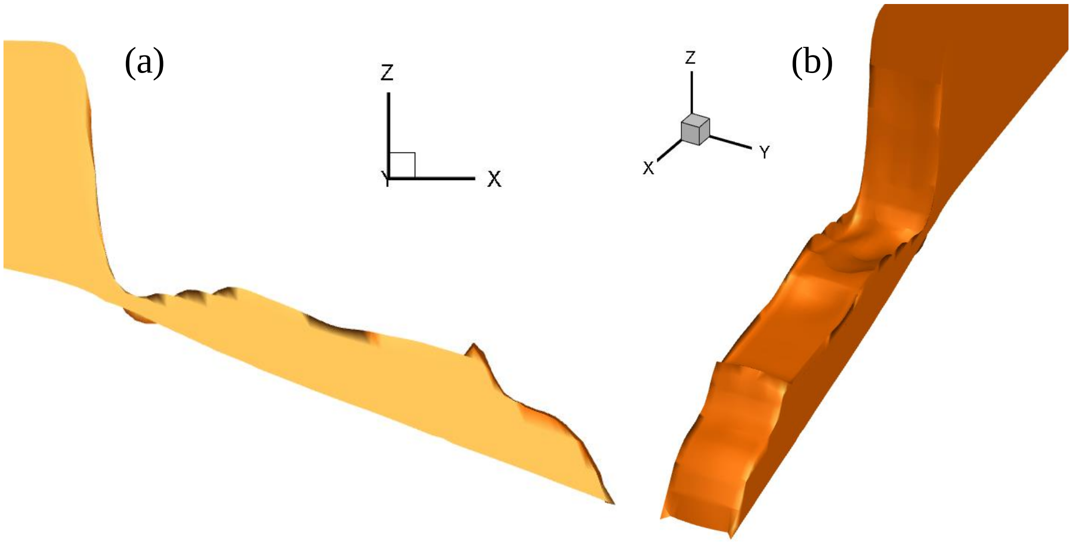

Figure 4.1: Side view (panel a) and an isometric view (panel b) of the iso-surface at $\rho = 1040$ kg/m^3 for simulation in a laterally confined channel.

4.2 3D Plunging Overview

To understand the plunge phenomenon in an unconfined domain, it is helpful to look at Figures 4.3 and 4.4. The figures depict a simulation for scenario 1, where the density of the inflow is 1041 kg/m^3. Figure 4.3 shows density iso-surfaces for $\rho = 1039.5$, 1039 and 1038 respectively, just as flow exits the channel. The figures illustrate that the dense inflow begins to spread out laterally from the base of the flow almost immediately after entering the unconfined domain. Hence, the plume starts collapsing and spreading along the y direction even before plunging in the x takes place. Also, it can be seen that the spread is greater for the iso-surface of a lower ρ value. This indicates that lateral mixing takes place in the fluid and as result, the density starts decreasing and the flow starts peeling away at the sides, leaving a dwindling core at the center.

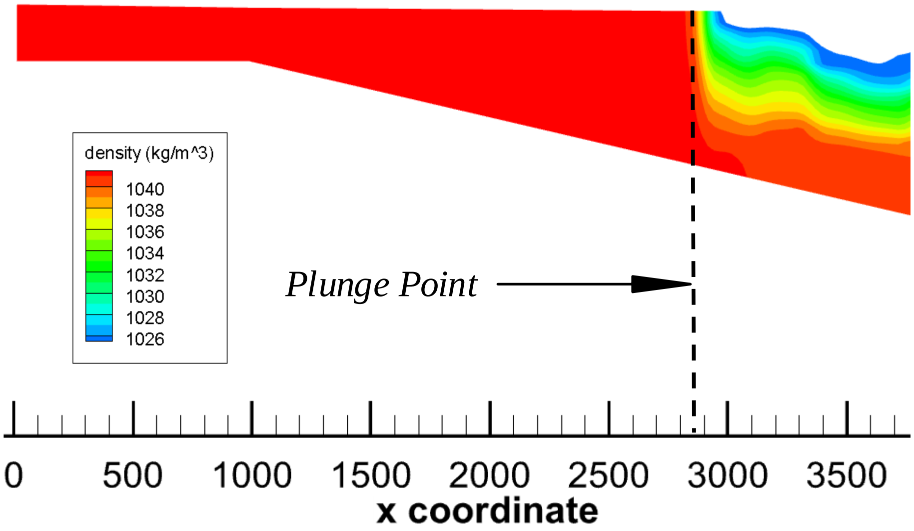

Figure 4.2: Density contours at the channel centerline for simulation in a laterally confined channel.

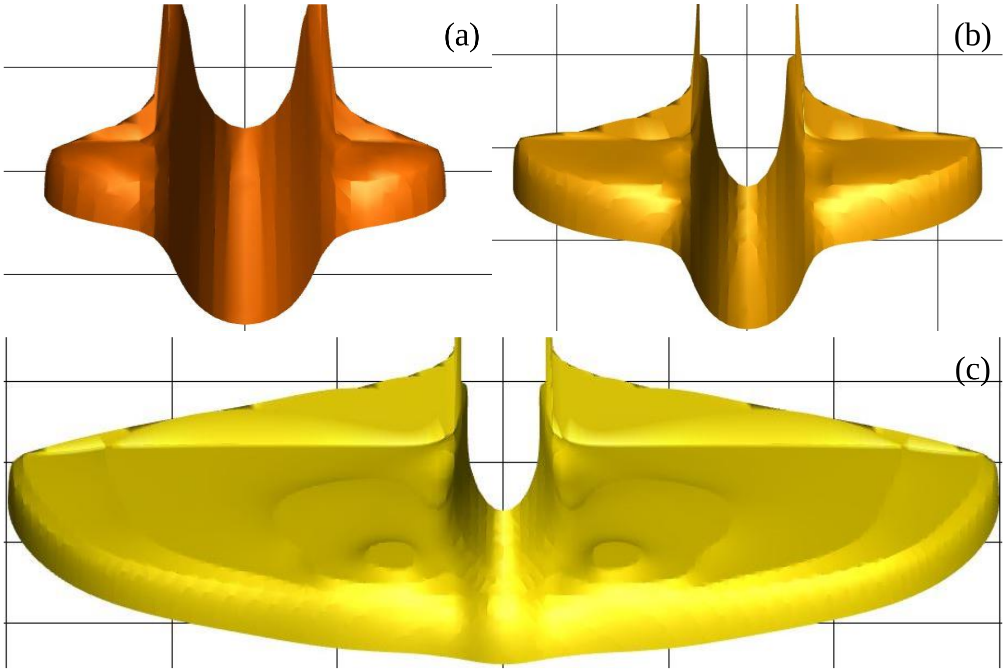

Figure 4.3: Iso-surfaces at $\rho = 1039.5$ (panel a), 1039 (panel b) and 1038 (panel c) kg/m^3 respectively for simulation 1.

Figure 4.4 shows density contours along the lateral direction at two locations: $x = 1015$ (15 meters into the domain) and $x = 1500$ (500 meters away from the channel mouth). It can be seen that the core of plume which has a high density is diminished as flow advances into the domain.

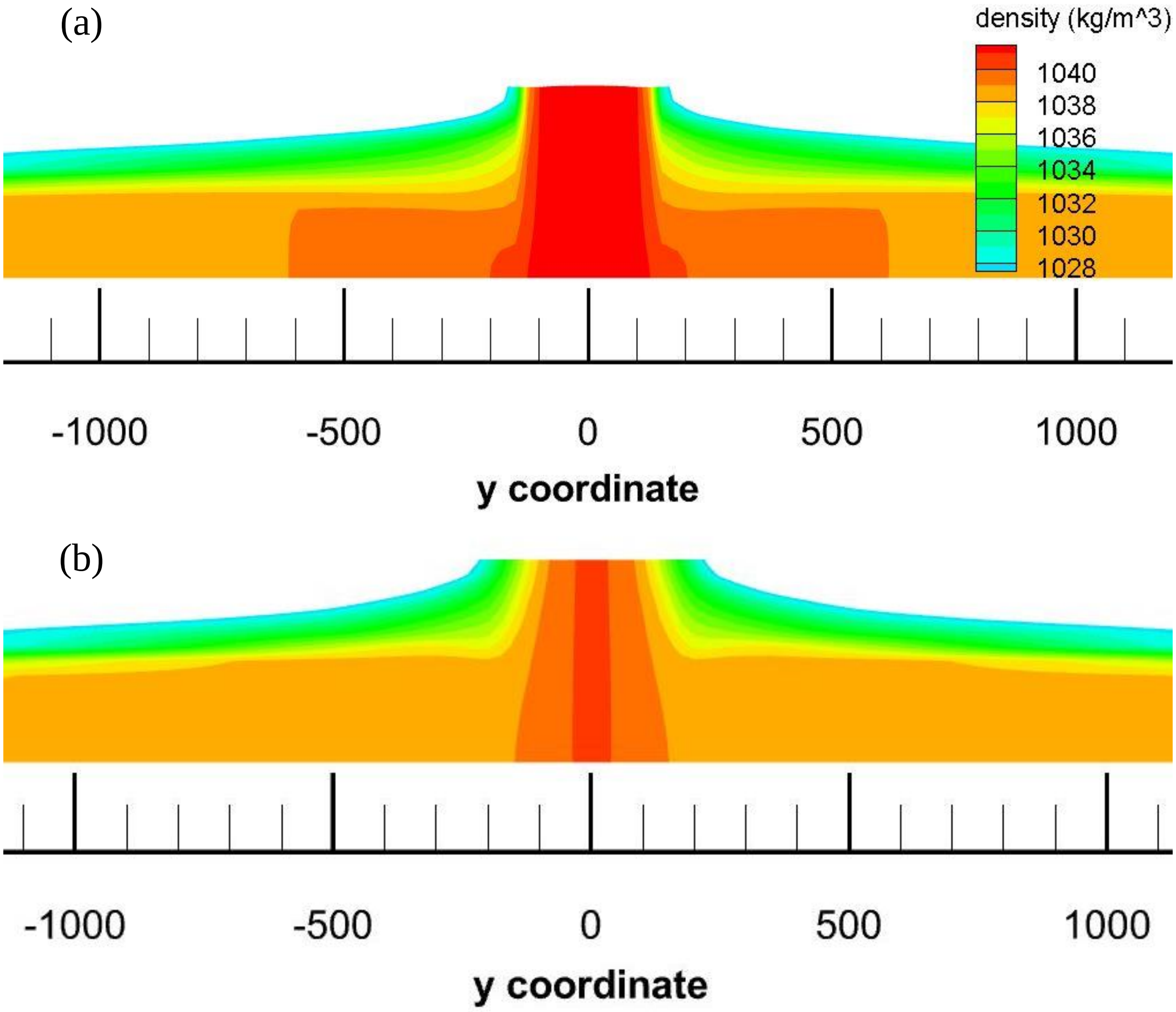

Figure 4.4: Density contours in the lateral direction at $x = 1015$ meters (panel a) and 1500 meters (panel b) for simulation 1.

4.3 Incipient Plunge Point

The incipient plunge location, calculated as per the definition in Section 2.4.1, is given in Tables 4.1 to 4.3 for all three density difference scenarios. In all cases, as the slope increases, the incipient plunge point moves closer to the river mouth. For scenarios 1 and 2 ($\Delta\rho = 18$), a slight change can be seen in the incipient plunge location with an increase in the Chézy friction coefficient (C_z) at lower slopes. The incipient plunge location is significantly greater (seaward) in case of scenario 3 ($\Delta\rho = 9$). As the density difference is less in this case, the velocity needs to be significantly reduced in order for the plume to plunge. Hence, the plume travels a longer distance before the density starts decreasing. Also, the values are consistent for the same density difference i.e. scenarios 1 and 2. For all parameters in this chapter, the results for scenarios 1 and 2 are similar as most of them depend on the density difference ($\Delta\rho$) and not the absolute density values. Hence to avoid repetition and confusion, the results will be discussed only for one of the two scenarios.

Slope	$C_z = 45$	$C_z = 55$	$C_z = 65$
0	1462.5	1237.5	1187.5
0.001	1212.5	1162.5	1137.5
0.003	1162.5	1137.5	1112.5
0.005	1137.5	1112.5	1112.5
0.01	1087.5	1087.5	1087.5
0.1	1037.5	1037.5	1037.5

Table 4.1: Incipient plunge point locations for Scenario 1.

4.4 Densimetric Froude number and plunge point

As discussed earlier (Section 2.4.2), location of the plunge point in the receiving basin is calculated by analyzing the centerline densimetric Froude number for each simulation. The plunge point is reported as the location where the densimetric Froude number reaches a

Slope	$C_z = 45$	$C_z = 55$	$C_z = 65$
0	1487.5	1237.5	1187.5
0.001	1212.5	1162.5	1137.5
0.003	1162.5	1137.5	1112.5
0.005	1137.5	1112.5	1112.5
0.01	1112.5	1087.5	1087.5
0.1	1037.5	1037.5	1037.5

Table 4.2: Incipient plunge point locations for Scenario 2.

Slope	$C_z = 45$	$C_z = 55$	$C_z = 65$
0	2437.5	2362.5	2462.5
0.001	1837.5	1862.5	1562.5
0.003	1337.5	1262.5	1237.5
0.005	1237.5	1187.5	1187.5
0.01	1162.5	1137.5	1137.5
0.1	1062.5	1062.5	1062.5

Table 4.3: Incipient plunge point locations for Scenario 3.

minimum value after the flow enters the basin before increasing again. Figures 4.5, 4.6 and 4.7 show the variation of plunge point location and the densimetric Froude number (Fr_d) at plunge for all three scenarios. For a better understanding, it is important to keep in mind that the channel mouth is located at (x) 1000 meters. Across all the scenarios, a similar trend of a closer plunge location is observed with an increase in bottom slope. However for a constant slope, the plunge location does not vary much with the Chézy friction coefficient. The critical Fr_d values at the plunge point range from 0.58 - 1.57 for scenarios 1 and 2. The model predicts higher Fr_d values at the plunge point for scenario 3. The results have been discussed in detail in Section 5.3.

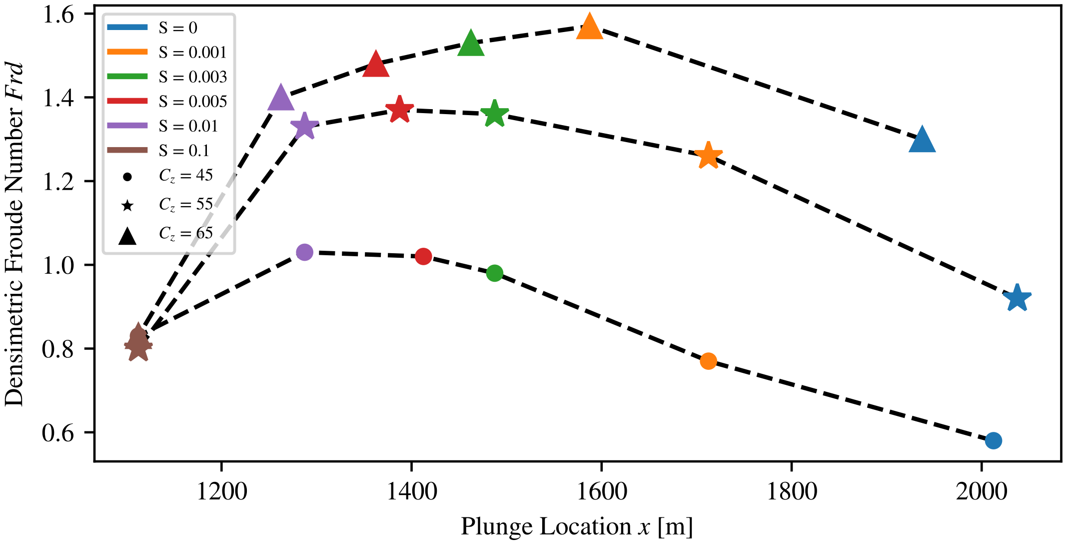

Figure 4.5: Densimetric Froude number Fr_d at plunge locations for Scenario 1

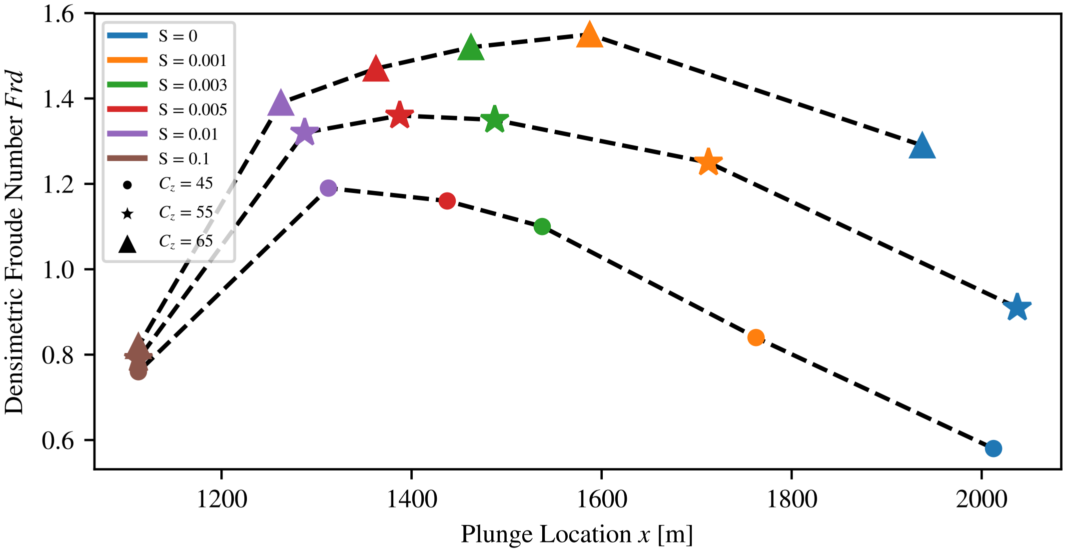

Figure 4.6: Densimetric Froude number Fr_d at plunge locations for Scenario 2

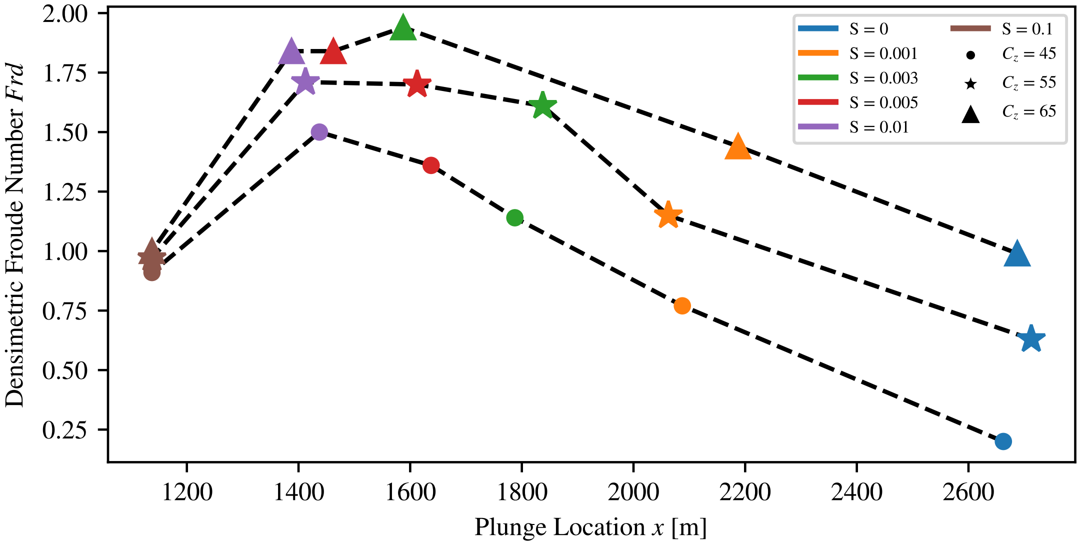

Figure 4.7: Densimetric Froude number Fr_d at plunge locations for Scenario 3

4.5 Plume Spreading

The width of the plume was calculated as described in Section 2.4.3. Hetland (2010) linked plume spreading with a rate of change of the plume width with. This research uses a plume spread rate given by

$$\frac{dW}{dx} = \frac{W_x - W_0}{x - x_0} \tag{4.1}$$

where W_x is the plume width at a location x from the river mouth and W_0 is the plume width at the river mouth x_0. The study by Hetland (2010) verified the plume spreading for a hypopycnal plume and found a relationship between the spread and the local Richardson number (R_i), which is given by equation A.13.

For this study, a similar calculation was used to compare the rate of plume spreading with Richardson number for the hyperpycnal case. Figure 4.8 shows the observations for spread rate (dW/dx) with respect to the $\sqrt{R_i}$ up to the plunge point, at all bottom slopes for scenario 1 with a Chézy coefficient (C_z) 45. Since all simulations follow a similar trend, plots for all three scenarios, with all friction coefficients have been included in the appendix B to avoid repetition. The plume spreading rate up to the plunge point reaches a constant value for all slopes, almost immediately after the flow exits the channel except for a horizontal bottom ($S = 0$). The figure illustrates that for this study, the spreading rate for hyperpycnal plumes in Zone 2 is not in agreement with the model developed for the hypopycnal case. However, a linear relationship is observed between the plume width (W) and $\sqrt{R_i}$ as shown in Figure 4.9.

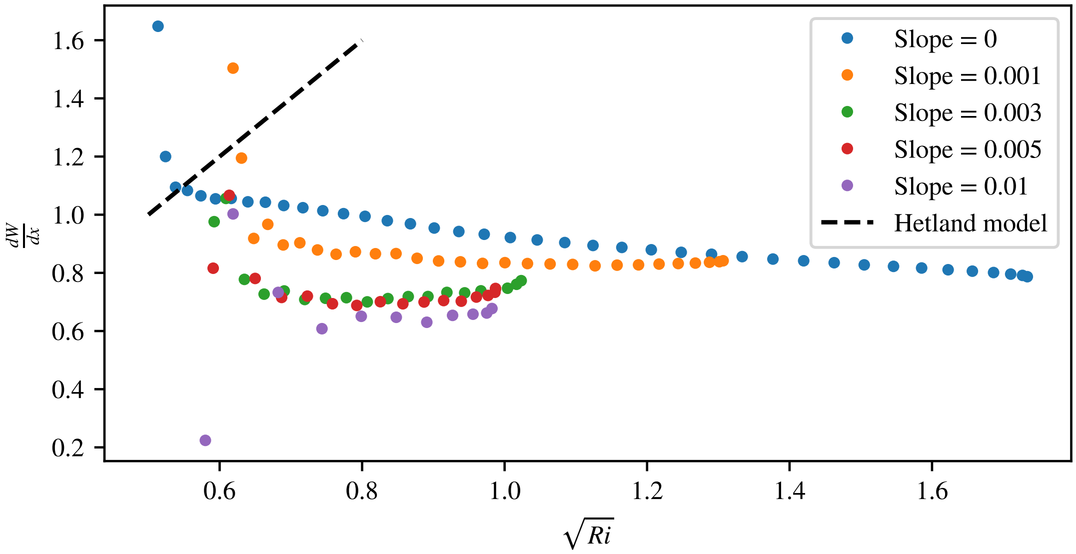

Figure 4.8: dW/dx for Scenario 1 ($C_z = 45$).

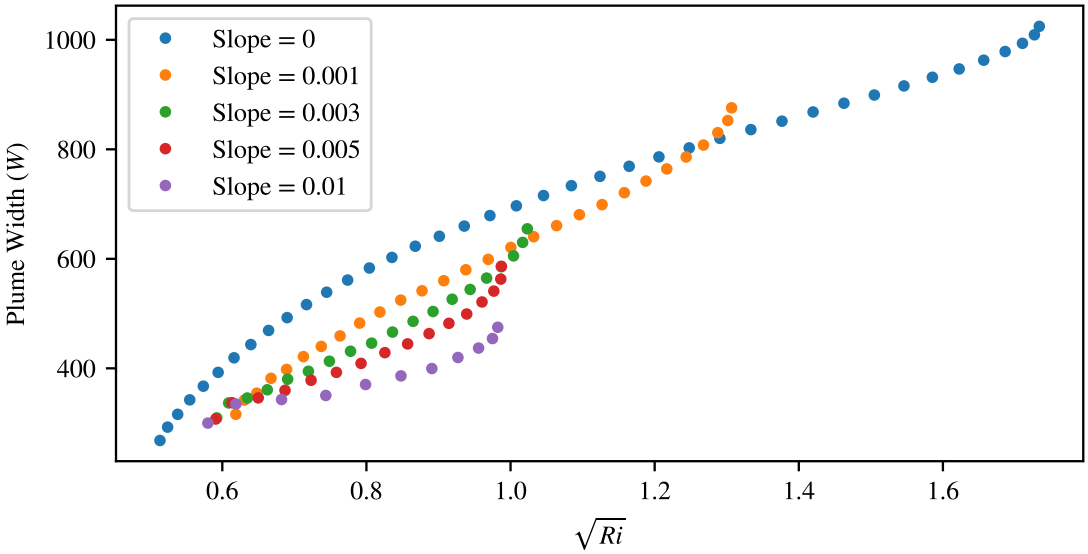

Figure 4.9: Plume width (W) for Scenario 1 ($C_z = 45$).

4.6 Comparison with the Jet Model and 2D plunging

As mentioned in Section 2.4.4, the plunge locations for all scenarios with density difference $\Delta\rho = 18$ were also calculated using the Jet Model and the 2D channel analysis. For both cases, the plunge point was located based on the critical $Fr_d = 1$. The assumption embedded in this calculation is that plunging of hyperpycnal flows occurs at the densimetric Froude number of unity, which is not necessarily the condition observed with the Delft3D model. Figures 4.10 and 4.11 give a comparison between the plunge locations as predicted by the jet model, the 2D analysis and that calculated with Delft3D.

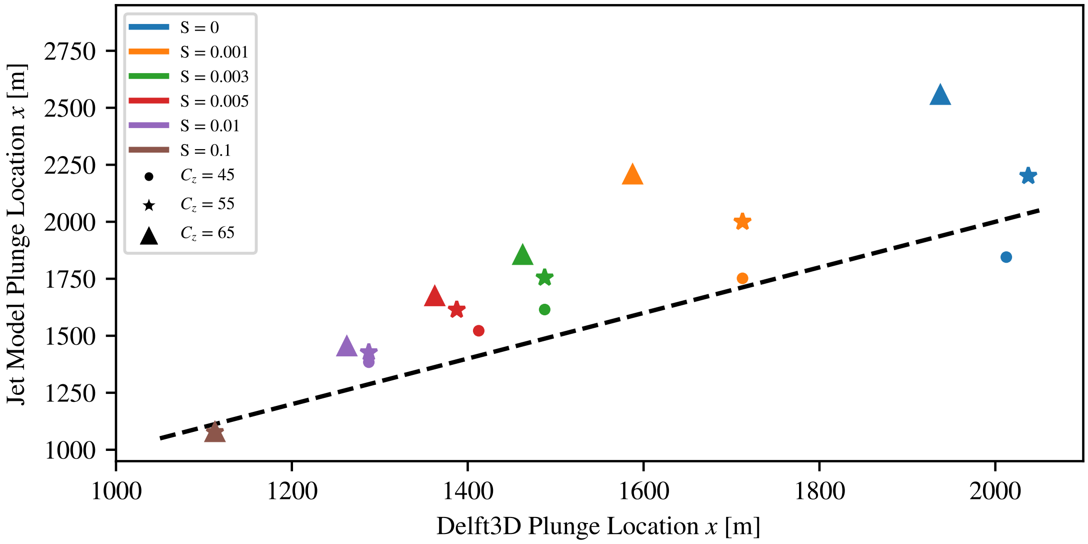

Figure 4.10: Plunge point comparison between Delft3D and the jet model. The dashed line is the 1:1 line of perfect correspondence.

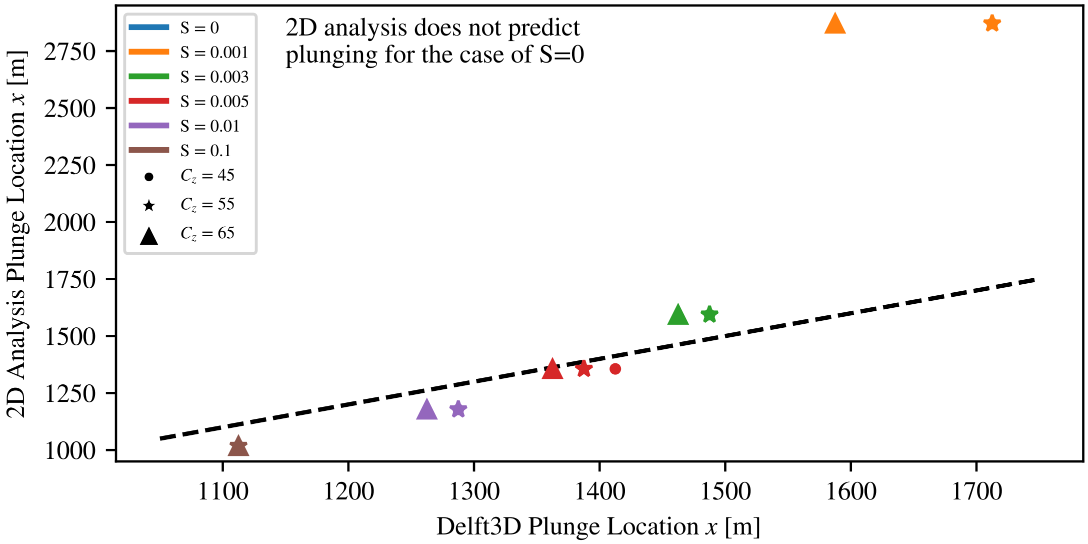

Figure 4.11: Plunge point comparison between Delft3D and the 2D analysis. The dashed line is the 1:1 line of perfect correspondence.

4.7 Comparison with confined channel plunging

As mentioned in Section 2.3.1, a set of simulations were also carried out for all conditions of slope and for a density difference $\Delta\rho = 18$, in case of a confined channel. The plunge point was calculated similar to the method defined in Section 2.4.2. Figure 4.12 shows comparison between the plunge locations calculated in the unconfined domain and that in case of the confined channel. The figure illustrates that for a same slope, the plunge point is further into the basin for simulations with a confined channel. This is further discussed in chapter 5.

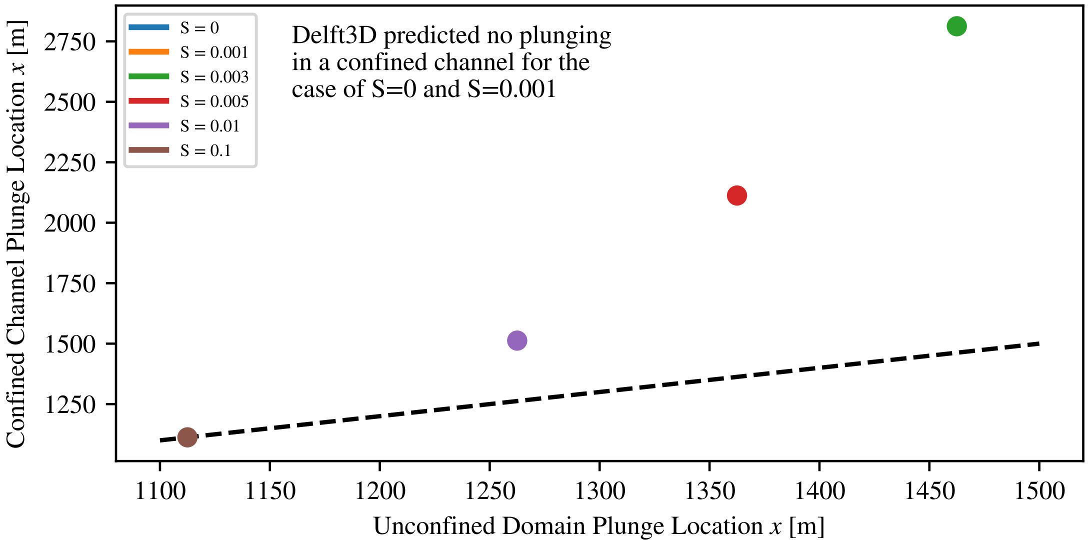

Figure 4.12: Plunge point comparison between the unconfined domain and the confined channel analysis. The dashed line is the 1:1 line of perfect correspondence.

Chapter 5

Discussion

5.1 Hypotheses

In answering the first research question, it was hypothesized that spreading occurs between the mouth and the plunge point (Zone 2) due to momentum diffusion and buoyant spreading. This can be seen from Figure 4.3, where spreading can be seen as soon as the flow enters the receiving basin. The plot of plume width up to the plunge point as shown in Figure 5.3 also supports the hypothesis that spreading takes place in Zone 2. Also, the analysis indicates that the cross shore location for plunging is changed when lateral spreading in Zone 2 is taken into account as opposed to the two dimensional depth limited plunging case. The results from our experimental simulations, in comparison with those from the jet model and 2D analysis, show that the plunge location as predicted by our analysis differs from that predicted by the jet model and the 2D analysis. This indicates that Delft3D accounts for some mechanisms or flow processes that have not been taken into consideration by the conventional analysis methods. Also, the jet model has initially been developed for a buoyant (hypopycnal) plume and our results demonstrate that it cannot be applied to the hyperpycnal case. More importantly, these experiments showed that when accounting for lateral spreading, the plunge point moves closer to the channel mouth as compared to that predicted by the jet model. However, in the case of 2D analysis, the relationship between the plunge location predictions are dependent on the basin slope. For low slopes, Delft3D predicts plunging closer to the mouth but there exists a critical slope at which the plunge point predictions are almost similar to that of the 2D model. At any slope greater than this critical value, the 2D model plunge point is closer to the mouth than its Delft3D counterpart.

In answering the second research question, it was hypothesized that the lateral spreading of the plume is affected by the basin slope (S), bottom friction (C_z) and the density difference ($\Delta\rho$) between the inflow and the ambient fluid. The rate of spread decreases with an increase in S, C_z and a decrease in ($\Delta\rho$). Analysis of the results indicate that spread rates do follow similar trends with different parameters (S, C_z and $\Delta\rho$) as hypothesized. Figure 4.8 shows a decrease in the spread rate with increasing slope S. Change in spread rate with the Chézy coefficient (C_z) for one slope ($S = 0.003$) can be seen in Figure 5.1 for scenarios 1 and 3. This is further discussed in a later section of this chapter. As you can see from Figure 5.2, the spread rate also changes for different $\Delta\rho$ scenarios. A decrease in $\Delta\rho$ results in a slight decrease in the rate of spread.

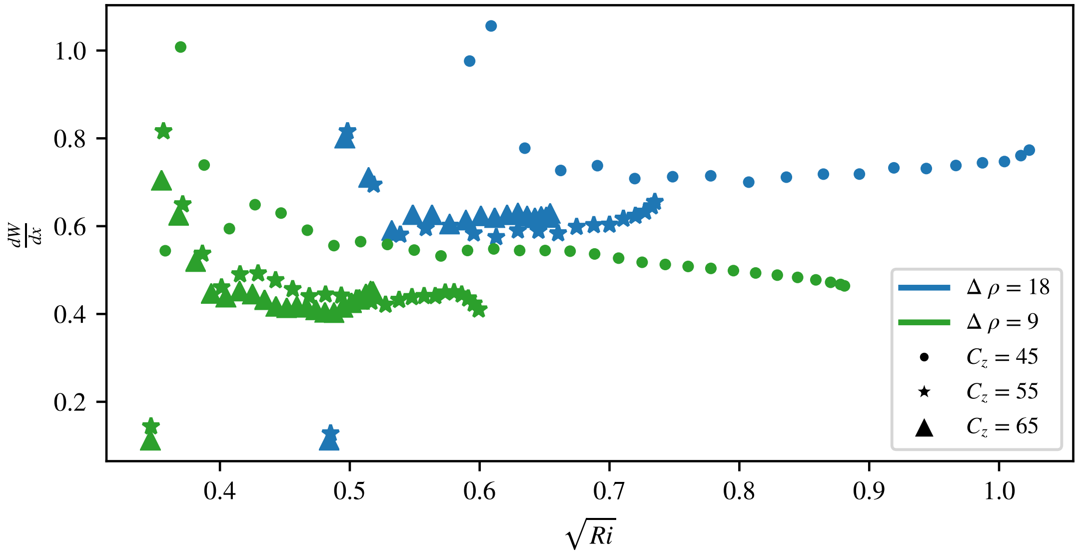

Figure 5.1: Plume spread rate for Scenarios 1 and 3, $S = 0.003$

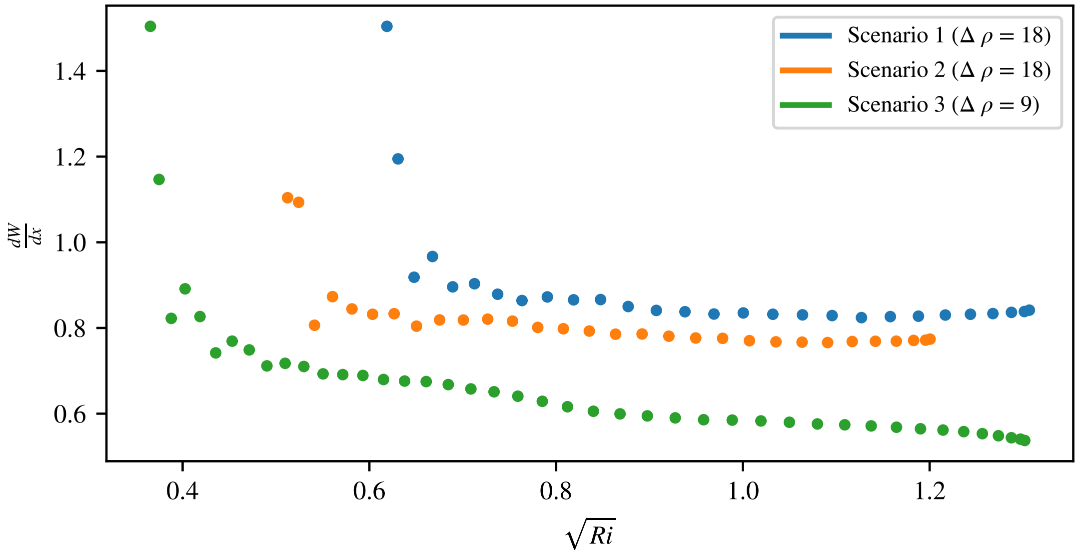

Figure 5.2: Plume spread rate for Scenarios 1, 2 and 3, ($S = 0.001$ and $C_z = 45$)

In answering the third research question, it was hypothesized that in the case of a hyperpycnal discharge, lateral buoyant spreading occurs between the river mouth and the plunge point (Zone 2) and the rate of spread is similar to that in a hypopycnal plume. That is, out of the two mechanisms responsible for spreading, buoyancy dominates and the rate of spread is dictated by the internal speed of the wave between the inflow and ambient water. However looking at the spread rate results, it is clear that the rate of spread for hyperpycnal flows is not similar to that in the hypopycnal case. This is further discussed in Section 5.4 of this chapter. However, the rate of increase in plume width is almost a constant value after flow exits the channel. This indicates that it seems to be momentum diffusion that dominates the plume spread in Zone 2.

In answering the fourth research question, it was hypothesized that plunging of a hyperpycnal plume occurs when the flow reaches a densimetric Froude number (Fr_d) of unity. This was mostly based on the available literature and the calculations involving the jet model and the 2D analysis (concept of depth limited plume). However, the results from this study do reveal that for a three dimensional analysis, a hyperpycnal flow does not necessarily plunge at $Fr_d = 1$. As reported by Tseng and Chou (2018), this study also finds plunging occurring at a range of Fr_d values (0.58-1.57). This is further discussed in Section 5.3.

5.2 Incipient Plunge Point

The incipient plunge point represents the location in the basin where the plume starts sinking underneath the ambient water. It can be seen as the point where the processes that lead to plunging begin. The incipient plunge locations along the x direction have been reported in Tables 4.1, 4.2, and 4.3. The values indicate that the incipient plunge locations are similar for simulations in scenario 1 and 2 and but that they differ significantly from those in scenario 3. This means that it is the density difference ($\Delta\rho$) between the inflow and ambient water that dictates how far the plume travels into the basin before it starts plunging and not the absolute density values themselves. Also, for all cases, the incipient plunge point moves closer to the channel mouth as the basin slope increases. However, not much difference is observed with changing friction coefficients (C_z), the only exception being for the case of horizontal bottom ($S = 0$), when the incipient plunge point is closer to the river mouth for higher friction coefficient (C_z) values.

5.3 Densimetric Froude number and plunge point

The plunge point in this study is considered to be the location at which the densimetric Froude number Fr_d reaches the minimum before rising again. At plunge point, flow in the bottom layer keeps advancing and at the same time, the velocity at the surface keeps decreasing. The plunge point locations and their corresponding critical densimetric Froude numbers for simulations in all three scenarios are shown in Figures 4.5, 4.6 and 4.7. For all

$\Delta\rho$ scenarios, the plunge point follows the same trend as that of the incipient plunge point, i.e. it gets closer to the channel mouth with increasing bathymetry slope. Also, the plunge locations predicted for all simulations with same density difference (scenarios 1 and 2) are similar. However, those for a lower density difference are significantly greater (seaward). This means that the higher the density difference between inflow and the ambient receiving water, the less the river water progresses into the basin before plunging. It can be seen that the plunge locations do not show a great difference with a change in the friction coefficient (C_z). This means that the basin slope has a greater influence on where the plume plunges than the bottom friction.

Across all scenarios, for lower basin slopes, the critical densimetric Froude number values corresponding to their respective plunge locations show a greater variation with changing friction whereas a less variation is observed for its counterparts with greater slopes. This makes sense because one would expect boundary friction to exert more influence on the dynamics in shallower flows. The Fr_d values are exactly similar for simulations in scenarios 1 and 2, and they are greater for the runs in scenario 3, only for cases with slopes of 0.003, 0.005 and 0.01. For scenario 3, the density difference ($\Delta\rho$) is less and an increase in Fr_d means that in those cases, $\Delta\rho$ is significantly reduced at plunging as the plunge point is located further away from the channel mouth. Also, the Fr_d goes on increasing with an increase in slope. This might be because as the slope increases, the plunge location shifts towards the channel and the velocity is greater closer to the channel mouth. This increase in Fr_d is sharp for lower friction coefficients. The values for Fr_d lie between 0.58 and 1.57 for scenarios 1 and 2, and between 0.63 and 1.84 for scenario 3. However, there is one case (simulation 3) for scenario 3 ($C_z = 45$, $S = 0$) where the Fr_d at plunge point is extremely low (0.2). It is important to note, that in all cases, for a very large slope ($S = 0.1$), the plume almost plunges immediately after leaving the channel and the corresponding Fr_d values are in close agreement with one another irrespective of the friction factor.

5.4 Plume Spreading

The main objective of studying hyperpycnal flows using a three dimensional hydrodynamic modeling software like Delft3D is to observe changes in the plume after the flow exits the channel. Hetland (2010) showed that the balance between mixing and spreading are dominant factors in controlling the plume structure. This study uses the definition of plume width (Section 2.4) as the main parameter to examine spreading. Figure 5.3 shows a plot for plume width as flow comes out of the channel into the unconfined domain. It can be seen that in all cases, the plume width begins increasing as the flow enters the basin which confirms spreading in the lateral direction.

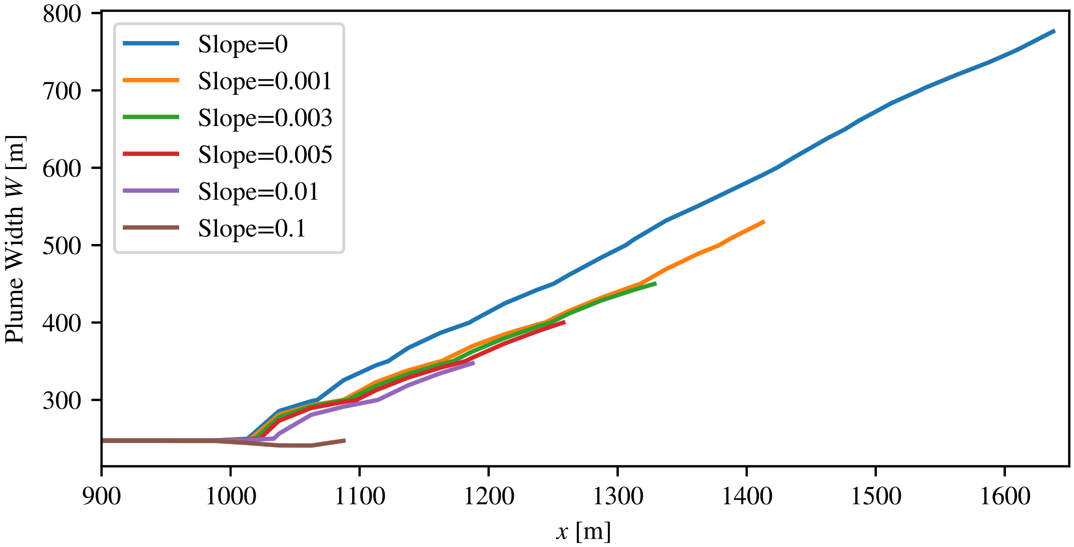

Figure 5.3: Plume width up to plunging as it exits the channel for Scenario 1 ($C_z = 65$)

To quantify plume spreading, a spread rate was determined using Equation 4.5 which represents change in plume width with respect to the channel width. The simulation conducted for hypopycnal case proved that the definition of width is in agreement with the results as predicted by the layer model (Hetland, 2010). The goal of this study was to check whether the layer model is also applicable to hyperpycnal studies. Results indicate that the rate of spread for a hyperpycnal plume does not follow the same trend as that of the buoyant plume (4.8). In comparison to the layer model, instead of increasing with $\sqrt{R_i}$, the rate of spreading reaches almost a constant value up to the plume plunge point. Immediately after the channel ends, due to a sudden change in the plume width, the first few spread rate values, at locations close to the mouth, show a larger deviation before quickly reaching a constant value. The behaviour of plume spreading can be attributed to the fact that in case of a negatively buoyant plume, the total flow depth (h) needs to be considered in the calculation of the Richardson number (R_i). It is important to note an observation that for all simulations conducted on a basin with a horizontal bottom ($S = 0$), there was a slight decrease in the rate of spread (dW/dx) with $\sqrt{R_i}$.

Results also show that the rate of spread is also dependent on the bottom slope and it decreases as the slope goes on increasing. This is analogous to the hypothesis that the lateral spreading of the plume decreases for a steeper bed slope. This trend holds true for all simulations irrespective of the friction coefficient or the density difference. The rate of spread is also slightly reduced when the Chézy coefficient is greater, but this variation is not as significant as that with basin slope. Also,Figure 5.2 illustrates that for a reduced density difference ($\Delta\rho = 9$) (scenario 3), the spread rate values are slightly lower, but the difference is not that significant, which indicates that spreading is not a function of the absolute values of the densities of flow or the density difference. This is an important observation as it implies that hyperpycnal flows do not require that there is a minimum density difference for plumes to spread before plunging. The analysis also revealed an important relationship between the plume width (W) and $\sqrt{R_i}$ (Figure 4.9). There exists a linear trend between (W) and $\sqrt{R_i}$, which follows similar trends with slope and friction as that followed by the rate of spread.

5.5 Comparisons with the Jet Model and 2D analysis

To highlight the three dimensional analysis by Delft3D, differences between the plunging predicted by the jet model, the two dimensional analysis and that predicted by Delft3D are discussed. Details of the analysis for jet model and 2D case are described in Section 2.4.4. As a result of lateral spreading, Delft3D predicts plunging closer to the channel mouth than that predicted by the jet model. This means that lateral spreading up to the plunge point does have an affect on the plunge location of the plume. The difference between the predicted plunge locations by both methods is greater for higher friction coefficients in all cases. However, there is one scenario for zero bed slope ($C_z = 45$) where the plunge location predicted by the jet model is closer to the river mouth.

Plunge locations for scenarios 1 and 2 are also calculated using the 2D analysis as mentioned in section 2.4.4. For simulations with a horizontal bottom, the 2D analysis predicted no plunging as opposed to the Delft3D model. Also, the 2D analysis predicted plunging closer to the basin for lower bottom slopes. However, there exists a cross over slope (S = 0.005) for which at any slope values greater than that cross over value, the 2D plume plunges earlier. In 2D analysis, a change in the friction coefficient has no effect on the plunge location. It is only the slope that changes the plunge point.

Both the jet model and the 2D analysis are based on the idea of a critical densimetric Froude number $Fr_{d,cr}$, which implies two criteria for plunging as discussed in Section 1.2. The fact that Delft3D predicts plunging even for simulations with a horizontal bottom ($S = 0$) rejects the idea that there needs to be a sufficient water depth that the flow must reach (the plunge depth, h_p) in order for it to plunge. Also, the densimetric Froude number (Fr_d) values observed at plunging range from 0.58-1.57 and 0.63-1.84 for scenarios with $\Delta\rho = 18$ and $\Delta\rho = 9$ respectively. This indicates that the criterion of $Fr_{d,cr}$, valid for laterally bound 2D channel flows is not applicable to plunging flows in an unconfined domain. Plunging observed across all three scenarios confirms that the only observable criterion that is necessary for plunging, according to this study is that the density of inflow must be greater than that of the ambient fluid ($\rho > \rho_a$).

5.6 Comparison with confined channel plunging

To highlight the effect of lateral spreading in an unconfined basin on the plunge location in the basin, simulations were also conducted in a laterally confined channel for all slopes as mentioned in Section 2.3.1. The comparison between their respective plunge points is shown in Figure 4.12. In case of a confined channel, the simulations did not predict plunging for slopes of 0 and 0.001 m/m as for these slopes, the flow did not reach a sufficient depth (h_p) for the depth limiting criterion to be satisfied. The figure also illustrates that for slopes greater than 0.001, the location of plunge in a confined channel is always further away from the river mouth. This means that the plume travels a longer distance before it plunges for a confined channel case. Thus, the plunge point moves closer to the river mouth when lateral spreading is taken into account. Also, for a very large slope of $S = 0.1$, the plunge point in the confined channel case is similar to that in case of the unconfined case and the plume plunges almost immediately after flow exits the channel.

Chapter 6

Conclusions

A series of numerical simulations were conducted in the Kelso Baker Environmental Hydraulics Laboratory at Virginia Tech to simulate negatively buoyant plumes in an unconfined domain using a three dimensional hydrodynamic software Delft3D. The simulations were conducted with different parameters of bottom slope (S), friction coefficient (C_z) and the density difference ($\Delta\rho$). These model runs and their results were then analyzed to determine the criterion that has the greatest influence on hyperpycnal flows. This study finds the following conclusions:

1. Flows with hyperpycnal potential will plunge irrespective of the density difference ($\Delta\rho$) between the inflow and ambient fluid.

2. Plunging of negatively buoyant plumes is observed even in case of a horizontal basin ($S = 0$). This impugns the idea of a depth limited plunge criterion that has been put forward from previous two dimensional analyses.

3. The plunge location (x_p) of a hyperpycnal plume is greatly affected by slope (S) of the receiving basin and the initial density difference ($\Delta\rho$) between the fluids. (x_p) moves closer to the river mouth with increasing S and $\Delta\rho$. The bed friction does not have a significant impact on the distance traveled by the plume before plunging.

4. The densimetric Froude numbers (Fr_d) at plunge range between 0.58-1.57. All three parameters S, C_z and $\Delta\rho$ influence the Fr_d at plunge.

5. The layer model developed by Hetland (2010) to quantify spreading of buoyant plumes is not applicable in case of hyperpycnal plumes. This study finds that for hyperpycnal flows, the plume spreads at a constant rate and that the rate of change in plume width (W) mainly depends on the basin slope (S).

6. The three dimensional analysis (Delft3D) that accounts for lateral spreading, predicts plunging closer to the river mouth as compared to that predicted by the jet integral model and simulations in a confined channel.

6.1 Future Work

The model built in this study, using Delft3D is capable of simulating the flow regimes that extend from laterally confined regions of a river in to an unconfined receiving basin of a lake, reservoir or an ocean. Delft3D can be a powerful tool in simulating density flows, both hypopycnal and hyperpycnal. More 3D studies and additional data is needed to determine the criteria that govern plunging and spreading of hyperpycnal plumes. In particular, more studies are needed in case of hyperpycnal flows that analyze plume spreading with the definition of plume width used in this thesis. This would serve an important purpose of verifying the plume width definition and also improving the understanding of plume spreading. Additional future work would also include developing a mathematical model that describes plume width as a function of Slope (S), density difference ($\Delta\rho$), and velocity (U).

Bibliography

Ahmed, D., Latrache, N., and Nsom, B. (2018). Mixing of saline gravity current jet into ambient freshwater in weakly turbulent regime. *Journal of Hydraulic Engineering.*

Akiyama, J. and Stefan, H. (1987). Onset of underflow in slightly diverging channels. *Journal of Hydraulic Engineering*, 113(7):825–843.

Akiyama, J. and Stefan, H. G. (1984). Plunging flow into a reservoir: Theory. *Journal of Hydraulic Engineering*, 110(4):484–499.

Alavian, V. (1986). Behavior of density currents on an incline. *Journal of Hydraulic Engineering*, 112(1):27–42.

Alavian, V., Jirka, G. H., Denton, R. A., Johnson, M. C., and Stefan, H. G. (1992). Density currents entering lakes and reservoirs. *Journal of Hydraulic Engineering*, 118(11):1464–1489.

Arita, M. and Nakai, M. (2008). Plunging conditions of two-dimensional negative buoyant surface jets released on a sloping bottom. *Journal of Hydraulic Research*, 46(3):301–306.

Bhattacharya, J. P. and MacEachern, J. A. (2009). Hyperpycnal rivers and prodeltaic shelves in the Cretaceous seaway of North America. *Journal of Sedimentary Research*, 79:184–209.

Bournet, P., Dartus, D., Tassin, B., and Vinçon-Leite, B. (1999). Numerical investigation of plunging density current. *Journal of Hydraulic Engineering*, 125(6):584–594.

Caldwell, R. L. and Edmonds, D. A. (2014). The effects of sediment properties on deltaic processes and morphologies: A numerical modeling study. *Journal of Geophysical Research: Earth Surface*, 119(5):961–982.

Chen, F., MacDonald, D. G., and Hetland, R. D. (2009). Lateral spreading of a near-field river plume: Observations and numerical simulations. *Journal of Geophysical Research: Oceans*, 114(C7).

Chen, S.-N., Geyer, W. R., and Hsu, T.-J. (2013). A numerical investigation of the dynamics and structure of hyperpycnal river plumes on sloping continental shelves. *Journal of Geophysical Research: Oceans*, 118(5):2702–2718.

Dai, A. and Garcia, M. H. (2010). Energy dissipative plunging flows. *Journal of Hydraulic Engineering*, 136(8):519–523.

Dallimore, C., Imberger, J., and Hodges, B. (2004). Modeling a plunging flow. *Journal of Hydraulic Engineering*.

Deltares (2018). *User Manual Delft3D-FLOW: Simulation of multi-dimensional hydrodynamic flows and transport phenomena, including sediments*. Deltares, Delft, The Netherlands, version: 3.15, revision: 55922 edition.

dong An, R. and Li, J. (2010). Characteristic analysis of the plunging of turbidity currents. *Journal of Hydrodynamics, Ser. B*, 22(2):274 – 282.

Edmonds, D. A., Hoyal, D. C., Sheets, B. A., and Slingerland, R. L. (2009). Predicting delta avulsions: Implications for coastal wetland restoration. *Geology*, 37(8):759–762.

El-Gawad, S., Cantelli, A., Pirmez, C., Minisini, D., Sylvester, Z., and Imran, J. (2012). Three-dimensional numerical simulation of turbidity currents in a submarine channel on the seafloor of the niger delta slope. *Journal of Geophysical Research*.

Ellison, T. H. and Turner, J. S. (1959). Turbulent entrainment in stratified flows. *Journal of Fluid Mechanics*, 6:423–448.

Fang, X. and Stefan, H. G. (1991). Integral jet model for flow from an open channel into a shallow lake or reservoir. Technical report, St. Anthony Falls Hydraulic Laboratory.

Fang, X. and Stefan, H. G. (2000). Dependence of dilution of a plunging discharge over a sloping bottom on inflow conditions and bottom friction. *Journal of Hydraulic Research*, 38(1):15–25.

Farrel, G. J. and Stefan, H. B. (1986). Buoyancy induced plunging flow into reservoirs and coastal regions. Technical report, St. Anthony Falls Hydeaulics Laboratory, University of Minnesota, Minneapolis.

Farrell, G. J. and Stefan, H. G. (1988). Mathematical modeling of plunging reservoir flows. *Journal of Hydraulic Research*, 26(5):525–537.

Ford, D. F. and Johnson, M. C. (1980). Field observations of density currents in impoundments. *Surface water impoundments, ASCE*.

Fukuoka, S., Fukushima, Y., and Nakamura, K. (1980). Study of the plunge depth interface form of density currents in a two-dimensional reservoir. In *Japan Society of Civil Engineers*.

Garcia, M. H. (1993). Hydraulic jumps in sediment-driven bottom currents. *Journal of Hydraulic Engineering*, 119(10):1094–1117.

Geyer, W. R., Hill, P. S., and Kineke, G. C. (2004). The transport, transformation and dispersal of sediment by buoyant coastal flows. *Continental Shelf Research*, 24(7-8):927 – 949.

Gu, R. and Chung, S. (1998). Reservoir flow sensitivity to inflow and ambient parameters. *Journal of Water Resources, Planning and Management*.

Hauenstein, W. and Dracos, T. (1984). Investigation of plunging density currents generated by inflows in lakes. *Journal of Hydraulic Research*, 22(3):157–179.

Hetland, R. D. (2010). The effects of mixing and spreading on density in near-field river plumes. *Dynamics of Atmospheres and Oceans*, 49(1):37 – 53.

Hetland, R. D. and MacDonald, D. G. (2008). Spreading in the near-field merrimack river plume. *Ocean Modeling*, 21(1–2):12 – 21.

Huang, H., Imran, J., and Pirmez, C. (2005). Numerical model of turbidity currents with a deforming bottom boundary. *Journal of Hydraylic Engineering*.

Imran, J., Kassem, A., and Khan, S. (2004). Three-dimensional modeling of density current: I. flow in straight confined and unconfined channels. *Journal of Hydraulic Research*.

Itakura, T. and Kishi, T. (1979). Study on the turbidity density current in a reservoir. *16th Symp., Science of Natural Disasters*.

Jiménez-Robles, A. M., Ortega-Sánchez, M., and Losada, M. A. (2016). Effects of basin bottom slope on jet hydrodynamics and river mouth bar formation. *Journal of Geophysical Research: Earth Surface*, 121(6):1110–1133.

Jirka, G., Doneker, R., and Hinton, S. (1996). User's manual for cormix: a hydrodynamic mixing zone model and decision support system for pollution discharges into surface waters.

Jirka, G. H. (2007). Buoyant surface discharges into water bodies. ii: Jet integral model. *Journal of Hydraulic Engineering*, 133(9):1021–1036.

Johnson, T., Ellis, C., Farrell, G., and Stefan, H. (1987). Negatively buoyant flow in a diverging channel. ii: 3-d flow field descriptions. *Journal of Hydraulic Engineering*, 113(6):731–742.

Johnson, T. R. and Stefan, H. G. (1988). Experimental study of density induced plunging flow into reservoirs and coastal regions. Project report no. 245, St. Anthony Falls Hydraulic Laboratory, University of Minnesota.

Jones, G. R., Nash, J. D., Doneker, R. L., and Jirka, G. H. (2007). Buoyant surface discharges into water bodies. i: Flow classification and prediction methodology. *Journal of Hydraulic Engineering*, 133(9):1010–1020.

K., L. (1960). Flow and stress near an interface between stratified liquids. *Physics of Fluids*.

Kan, K. and Tamai, N. (1981). On the plunging point and initial mixing of the inflow into reservoirs. In *25th Japanese Conference on Hydraulics*.

Kassem, A. and Imran, J. (2004). Three dimensional modeling of density current: Ii. flow in sinuous confined and unconfined channel. *Journal of Hydraulic Research*.

Kassem, A. and Imran, J. (July, 2001). Simulation of turbid underflows generated by the plunging of a river. *Geology*, 29(7):655–658.

Kassem, A., Imran, J., and Khan, J. A. (2003). Three-dimensional modeling of negatively buoyant flow in diverging channels. *Journal of Hydraulic Engineering*, 129(12):936–947.

Khan, S. M., Imran, J., Bradford, S., and Syvitski, J. (2005). Numerical modeling of hyperpycnal plume. *Marine Geology*, 222-223:193 – 211.

Kilcher, L. F., Nash, J. D., and Moum, J. N. (2012). The role of turbulence stress divergence in decelerating a river plume. *Journal of Geophysical Research: Oceans*, 117(C5).

Lamb, M. P., McElroy, B., Kopriva, B., Shaw, J., and Mohrig, D. (2010). Linking river-flood dynamics to hyperpycnal-plume deposits: Experiments, theory, and geological implications. *Geological Society of America Bulletin*, 122(9/10):1389–1400.

Lamb, M. P. and Mohrig, D. (2009). Do hyperpycnal-flow deposits record river-flood dynamics?. *Geology*, 37(12):1067 – 1070.

Lee, H. and Yu, W. (1997). Experimental study of reservoir turbidity current. *Journal of Hydraulic Engineering*, 123(6):520–528.

MacDonald, D. G. and Geyer, W. R. (2004). Turbulent energy production and entrainment at a highly stratified estuarine front. *Journal of Geophysical Research*, 109(C5):C05004.

MacDonald, D. G., Goodman, L., and Hetland, R. D. (2007). Turbulent dissipation in a near-field river plume: A comparison of control volume and microstructure observations with a numerical model. *Journal of Geophysical Research*, 112(C07026).

Milliman, J., Lin, S., Kao, S., Liu, J., Liu, C., Chiu, J., and Lin, Y. (September, 2007). Short-term changes in seafloor character due to flood-derived hyperpycnal discharge: Typhoon Mindulle, Taiwan, July 2004. *Geology*, 35(9):779–782.

Mulder, T. and Syvitski, J. P. M. (1995). Turbidity currents generated at river mouths during exceptional discharges to the world oceans. *Journal of Geology*, 103(3):285–299.

Nakajima, T. (2006). Hyperpycnites deposited 700 km away from river mouths in the Central Japan Sea. *Journal of Sedimentary Research*, 76:60–73.

Olariu, C., Bhattacharya, J. P., Leybourne, M. I., Boss, S. K., and Stern, R. J. (2012). Interplay between river discharge and topography of the basin floor in a hyperpycnal lacustrine delta. *Sedimentology*, 59(2):704–728.

Parker, G. and Toniolo, H. (2007). Note on the analysis of plunging of density flows. *Journal of Hydraulic Engineering*, 133(6):690–694.

Robles, A. and Sanchez, M. (2018). Implications of river discharge angle and basin slope on mouth bar morphology and discharge dynamics of stable jets. *Journal of Hydraulic Engineering*.

Savage, S. B. and Brimberg, J. (1975). Analysis of plunging phenomena in water reservoirs. *Journal of Hydraulic Research*, 13(2):187–205.

Schuch, F. N., Pinto, L. C., Silvestrini, J. H., and Laizet, S. (2018). Three-dimensional turbulence-resolving simulations of the plunge phenomenon in a tilted channel. *Journal of Geophysical Research: Oceans*.

Singh, B. and Shah, C. R. (1971). Plunging phenomenon of density currents in reservoirs. *LaHouille Blanche*, 26(1):59–64.

Siqueira, A., Fiedler, M., and Yassuda, E. (2018). Delft3d morphological modeling downstream of sergio motta reservoir dam. *Springer Nature Switzerland*.

Stefan, H. G. and Johnson, T. R. (1989). Negatively buoyant flow in diverging channel. iii: Onset of underflow. *Journal of Hydraulic Engineering*, 115(4):423–436.

Strom, K. and Bhattacharya, J. P. (2012). Plunge location of sediment driven hyperpycnal river discharges considering bottom friction, lateral entrainment, and particle settling. In *American Geophysical Union, Fall Meeting 2012, abstract EP32A-0795*, San Francisco, CA.

Strom, K. and Keyvani, A. (2016). Flocculation in a decaying shear field and its implications for mud removal in near-field river mouth discharges. *Journal of Geophysical Research: Oceans*, 121:2142–2162.

Tseng, C.-Y. and Chou, Y.-J. (2018). Nonhydrostatic simulation of hyperpycnal river plumes on sloping continental shelves: Flow structures and nonhydrostatic effect. *Ocean Modelling*, 124:33 – 47.

Üneş, F. (2008). Analysis of plunging phenomenon in dam reservoirs using three-dimensional density flow simulations. *Canadian Journal of Civil Engineering*, 35(10):1138 – 1151.

Wang, H., Bi, N., Wang, Y., Saito, Y., and Yang, Z. (2010). Tide-modulated hyperpycnal flows off the Huanghe (Yellow River) mouth, china. *Earth Surface Processes and Landforms*, 35(11):1315–1329.

Wang, H.-W., Kondolf, M., Tullos, D., and Kuo, W.-C. (2018). Sediment management in taiwan's reservoirs and barriers to implementation. *Water*, 10(8).

Warrick, J. A. and Milliman, J. D. (September, 2003). Hyperpycnal sediment discharge from semiarid southern California rivers: Implications for coastal sediment budgets. *Geology*, 31(9):781–784.

Warrick, J. A., Xu, J., Noble, M. A., and Lee, H. J. (2008). Rapid formation of hyperpycnal sediment gravity currents offshore of a semi-arid california river. *Continental Shelf Research*, 28(8):991 – 1009.

Wright, L. and Friedrichs, C. (2006). Gravity-driven sediment transport on continental shelves: A status report. *Continental Shelf Research*, 26(17-18):2092 – 2107.

Wright, L. D. and Coleman, J. M. (1971). Effluent expansion and interfacial mixing in the presence of a salt wedge, Mississippi River Delta. *Journal of Geophysical Research*, 76(36):8649–8661.

Wright, L. D. and Coleman, J. M. (1974). Mississippi river mouth processes: Effluent dynamics and morphologic development. *The Journal of Geology*, 82(6):751–778.

Yu, W., Lee, H., and Hsu, S. (2000). Experiments on deposition behavior of fine sediment in a reservoir. *Journal of Hydraulic Engineering*, 126(12):912–920.

Yuan, Y. and Horner-Devine, A. R. (2013). Laboratory investigation of the impact of lateral spreading on buoyancy flux in a river plume. *Journal of Physical Oceanography*, 43(12):2588 – 2610.

Appendices

Appendix A

Review of Literature

Further background from literature is given below regarding what is known about the plunge phenomenon. This chapter presents some fundamental concepts as well as results from some experimental studies conducted to characterize the plunge. The first section of this chapter is dedicated to understanding the concept and the physical process of the plunge phenomenon. Most of the work discussed in the second section of this chapter consists of two dimensional analytical studies conducted inside laterally confined laboratory flumes. Appendices A.3 and A.4 delve into some of the initial three dimensional studies undertaken to study the plume, most of which include studies on hypopycnal plumes.

A.1 The physics behind plunging

The physical concept of plunging was first explained by Singh and Shah (1971), using the concept of eddy diffusion and displacement. Their study was carried out in a flume with clear tap water in the reservoir or the receiving basin and colored salt water was introduced as stream flow. The experiments included visual observations of the process of formation of the plunge point and after a steady plunge point was established, the location, depth and density were recorded at that point. The physical concept of plunging as put forward by Singh and Shah (1971) can be understood with the help of Figure A.1.

The surface of separation of flow, which occurs as a result of the density difference, is the interface between the incoming salt water and the clear tap water in the reservoir.

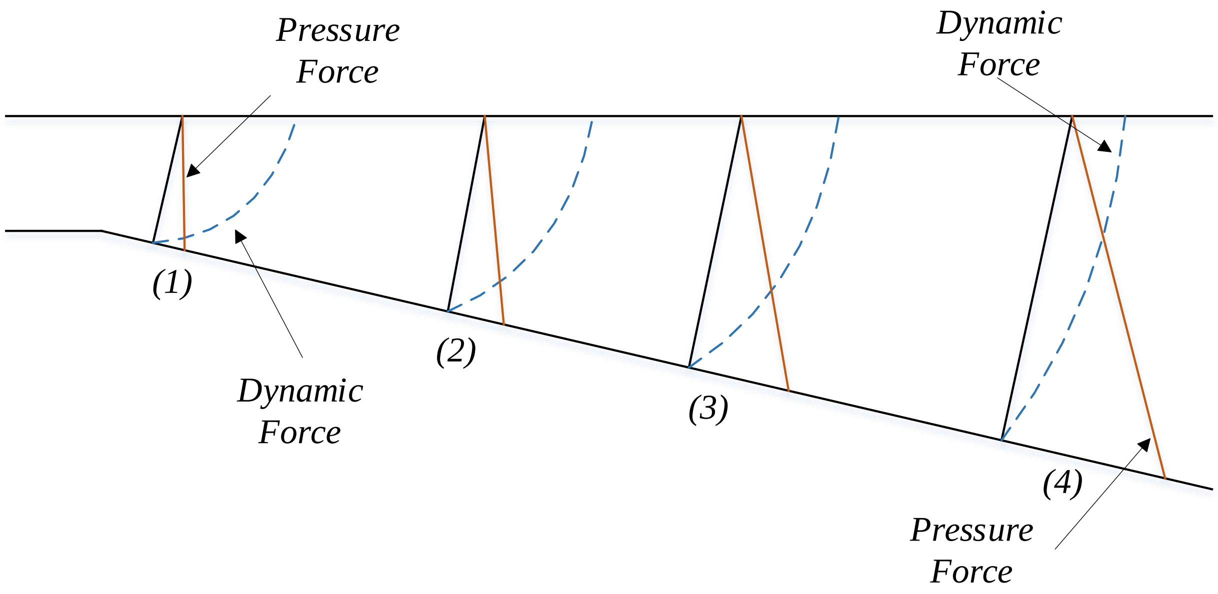

Figure A.1: Action of dynamic force and pressure force to form an underflow and a plunge point

It is acted upon by two driving forces and one resisting force. The two driving forces are (i) the dynamic force exerted by the inflow water due to its high momentum and (ii) the static force due to pressure gradient across the surface of separation. The pressure force will have zero magnitude at surface and will be maximum at the bottom. The dynamic force would have the exact opposite trend. The final shape and position of the surface of separation would be determined by the net effect of these forces. A stable position would be reached when these forces are balanced. The dynamic force at a point along the surface of separation is a function of the mass flow rate and the flow velocity whereas the pressure force depends on the density difference $(\rho_m - \rho_a)$ and the flow depth. Initially, the dynamic forces dominate the pressure forces due to low depth and high flow velocity. As the dense flow moves downstream, the depth increases and the velocity of flow decreases and therefore the influence of dynamic force will go on reducing. Meanwhile, at a certain point, the pressure forces will be significantly greater than the dynamic force and it would cause the flow at the bottom to advance, forming a density current. At this point, the velocity at surface would be relatively smaller and the point of contact of the surface of separation with the free surface would now be seen as a plunge point because of the density current moving at the bottom. The stability of the plunge point depends on the stable position of the interface, which depends on the balance of forces. In contrast, if there was no density difference between the river inflow and the receiving basin, there would not be any pressure forces and the surface of separation would move only as a result of the dynamic forces. In this case, there would be no underflow and the flow would occur at maximum velocity without a plunge.

A.2 Background

Much research has been done to experimentally examine the phenomenon of plunging, both hypopycnal and hyperpycnal. Most of the initial studies regarding hyperpycnal plunging were experimental simulations inside laboratory flumes (Akiyama and Stefan, 1984, 1987; Fang and Stefan, 2000). A key element of these studies was to demonstrate plunging of high density flows and predict plunge location and the depth at plunging. Other work has also shown that plunging of density flows is related to the lateral entrainment of ambient fluid (Huang et al., 2005) spreading (Alavian, 1986; Robles and Sanchez, 2018).

Along with providing a physical explanation to the phenomenon, the early work of Singh and Shah (1971) also introduced the concept of a depth limited plume, which basically states that for a hyperpycnal flow to plunge, there needs to be a certain minimum depth required and in cases where this required depth is not available, it creates a criterion of minimum density difference ($\Delta\rho$) for the formation of a stable plunge point. They also stated that deposition of suspended load would increase up to the plunge point and immediately after, the formation of a uniform density current would maintain the concentration of suspended load. This results in formation of an alluvial cone and not the other way around, which was a usually accepted reverse theory.

Akiyama and Stefan (1984) analyzed plunging flow by employing a set of integral equations consisting of the conservation of mass, volume and momentum. Their model accounted for mixing between the inflow and ambient water using two mechanisms: entrainment due to instability of the interface and mixing due to abrupt change in flow depth. Thus the bed slope of the channel (S) and becomes an important physical parameter controlling the plunge phenomenon. They also defined a mixing coefficient (γ), given by

$$\gamma = u_a \frac{h_a}{q_0} \tag{A.1}$$

as an important physical parameter controlling plunging where u_a is the ambient velocity, h_a is the depth of the ambient fluid flow and q_o is the initial unit discharge. Their model did a good job of matching the plunge depths with experimental results and field data available at the time. However, there were some inherent assumptions in the model which required the inflow rate (q_0) channel width (b) and slope (S) to be constant within the modeled reach. Also the reservoir was assumed to be completely mixed in the vicinity of plunging. Parker and Toniolo (2007) later noted that the basic structure of this analysis was sufficient to specify all relevant parameters concerning plunging as functions of the mixing coefficient (γ).

Building up on the study by Akiyama and Stefan (1984), Alavian (1986)'s analysis indicated that the dense layer spreads in all directions when he investigated the behaviour of salt solution released down a sloping surface in a tank of freshwater. This was the first study where a plunging inflow and the resulting flow along the bottom (density current) was investigated considering a three dimensional lateral spreading. The model developed emphasized on the flow geometry, entrainment and bottom friction along with the bottom slope and introduced the plume's dependence on Buoyancy Flux given by

$$B = \frac{\Delta\rho}{\rho_a} AU \tag{A.2}$$

where A cross sectional area of the dense layer which accounts for the plume geometry and U is the mean layer velocity. This study achieved an important feat of bridging the gap between two other studies, Ellison and Turner (1959) and K. (1960), by showing a continuity between the entrainment coefficient and the Richardson number. Following his study, Akiyama and Stefan (1987) also conducted experiments with diverging channels at different divergence angles to simulate buoyancy driven plunging flows. Their observations revealed a linear relation between maximum entrainment rates and the channel divergence angle and also the dependence of densimetric Froude number at the plunge line on the divergence angle.

Fang and Stefan (2000) noted that so far, performing a bulk analysis using momentum and continuity principles was applied to get results that were of immediate use in water quality modeling. A system was developed by Jirka et al. (1996) to analyze and predict pollutant discharges into diverse water bodies. However, it could not be applied to a discharge from a channel over a sloping bottom. Gu and Chung (1998) performed a sensitivity analysis for their two dimensional negatively buoyant flow from a shallow channel over a mildly sloping bottom into a stratified reservoir and concluded that the channel aspect ratio has no effect on plunging depth and the distance to plunging.

Fang and Stefan (2000) proposed the use of a previously verified (Fang and Stefan, 1991) slot integral jet model for discharges from a sudden open channel expansion over a horizontal sloping bottom to determine dilution up to plunging for application as an initial condition for density current operations. The equations developed provided a simple way to predict the distance to plunging and the dilution of negatively buoyant inflows for very large diffuser angles ($\delta > 45°$). However, their numerical predictions could not reproduce the experimental results (Fang and Stefan, 1991) ignoring bottom friction.

A two dimensional analysis of the plunging phenomenon was carried out by Kassem and Imran (2001), when they simulated the entire process of plunging, generation of turbid flows and the dynamics of the head of a turbidity current by solving the Reynolds-averaged Navier-Stokes (RANS) equations and conservation equations of suspended sediment in a conservative form, using a robust computational fluid dynamics solver (FLUENT, 1998) which treats the turbidity current and the ambient flow as a mixture of species. Their study was applicable to cases where only longitudinal and vertical spreading is considered. Closure of the turbulence stress term was obtained using the $k - \epsilon$ model. For a field scale test, the model was used to simulate a turbidity current in Saguenay fjord, Canada. The plunge location and depth agreed closely with the semi-empirical formulae described by (Akiyama and Stefan, 1984).

A.3 3D Plunging Studies

Dallimore et al. (2004) coupled a 2D underflow model (based on Bradford and Katapodes 1999) and a 3D lake model (Hodges et al. 2000), part of the Center for Water Research Estuary and Lake Computer Model (CWR-ELCOM) code to model plunging inflows accounting for the effects of the barotropic term before plunging. The inclusion of barotropic term indicates that the underflow is not always assumed to be beneath the less dense ambient water. This is important when the plunge point is located some distance into the receiving basin. They argued that in 2D integral models where the barotropic terms are assumed negligible compared to the baroclinic terms, the approach is strictly applicable to flows entirely submerged beneath the ambient fluid. This holds true for a case where the plunge point lies within the channel. However, the plunge point is generally some distance into the receiving water body and hence barotropic forcing must be incorporated in a general integral model.

The model's ability to capture a plunging inflow with variable bathymetry and inflow conditions was confirmed when their simulated results matched with the measured data for an inflow event in the Wellington Reservoir, Western Australia.

Density currents had been extensively studied by Kassem et al. (2003), Imran et al. (2004) and Kassem and Imran (2004) using FLUENT, a commercially available three dimensional hydrodynamic model. Khan et al. (2005) developed a numerical model 'Hyper' to investigate the effects of an alongshore current on the shape and direction of the turbid underflows. A flooding event on River Tronto, Italy was considered and the results indicated that the hyperpycnal plume moves towards the downstream direction following the natural gradient in the absence of alongshore current. Whereas, a southward alongshore current significantly changed the spreading pattern of the hyperpycnal plume. This study also carried out numerical experiments to study the evolution of bed features after a series of hyperpycnal events and results showed a possibility of the formation of complex channel-levee system with undulations. Huang et al. (2005) employed a similar model and successfully simulated the evolution of turbidity currents in a sloping flume followed by a horizontal bottom. They reported a strong influence of ambient water entrainment into the density current on the overall flow characteristics. The water entrainment coefficient (e_w) is defined by

$$e_w = \frac{1}{U}\frac{d(Uh)}{dx} \tag{A.3}$$

where U is the depth averaged velocity and h is the density current thickness. Their study observed that the Richardson number and the entrainment coefficients provided by their simulations simulations fell within the range of experimental data.

A similar study was carried out by El-Gawad et al. (2012), where a three dimensional model solving the RANS equations, along with a two equation turbulence closure model was employed to simulate turbid currents in the Niger Delta. This was one of the very first studies conducted on a large scale submarine environment. The two closure equations were the sediment conservation equations for multiple grain size classes and the Exner equation of bed sediment conservation. The model did realistically predict the flow of turbidity currents over complex seafloor topography.

An important study investigating the spreading of buoyant plumes was carried out by Hetland and MacDonald (2008) in which they found that plume properties are a function of their radial distance from the mouth and the spreading is related to the local internal gravity speed. Their study used the Regional Ocean Modeling System (ROMS) to simulate the near-field Merrimack River plume. Numerical drifters were introduced in the flow field and local plume spreading was observed from the drifter paths. The local spreading rate, which describes the rate at which two neighboring streaklines diverge, does not give the information about spreading of plume as a whole (Hetland and MacDonald, 2008). Hence a global spreading rate is defined, which is related to the two edges of the plume.

The relationship between lateral spreading and mixing in stratified gravity currents was first investigated by Yuan and Horner-Devine (2013). They conducted a series of experiments in laterally confined as well as unconfined channels. A freshwater inflow, dyed with colored food dye, was introduced at different flow rates and the plume width was measured using the Optical Thickness Method (OTM). It measures the mean plume freshwater thickness corresponding to the intensity of light transmitted through a distance (h_e) of fluid with dye concentration (C_0). The lateral distribution of h_e was described by a centralized Gaussian fit and the plume width was defined in terms of the standard deviation of the Gaussian fit ($b = 4\sigma$). Lateral spreading significantly modifies the plume's vertical structure. However, the results do not necessarily support that lateral spreading increases local mixing. The authors try to explain this with two possible mechanisms both of which refer to an idea of vertical structure to the spreading and mixing processes. In the region near the river mouth, as current moves offshore, the density and velocity profiles change drastically from two-layer step-wise profiles to mixing layer profiles. In this transition region, spreading occurs preferentially in the near-surface uniform density layer while mixing occurs at the lower layer of the plume and this mixing layer does not experience significant spreading. Further from the jet-to-plume region, the spreading plumes are characterized by linear density and velocity profiles. Here, the horizontal pressure gradient is expected to be a linear function of depth within the plume, maximum at the water surface and zero at plume base. In their experiments and also in studies of MacDonald and Geyer (2004), the lateral spreading rate was assumed to be independent of depth and this assumption agrees reasonably with experimental data even though the authors have related the discrepancies to the depth dependence of spreading.

The dynamics and structure of hyperpycnal plumes was studied over a sloping continental shelf, also using ROMS, a 3-D hydrodynamic model, by Chen et al. (2013) wherein the plume's response to changing slopes and settling velocities after plunging was the focal point of this study. They classify hyperpycnal plumes into three regimes: decelerating, autosuspending and accelerating based on the difference between upward turbulent lift and downward settling. The authors also argue that while hyperpycnal plumes follow the same dynamics as turbidity currents, they are driven by a weaker gravitational force for the same sediment suspension and are mainly fine grained (Warrick et al., 2008). Hence, self acceleration is unlikely to occur in hyperpycnal plumes due to lack of erodible mud on the continental shelf. The model was validated by comparing the predicted vertical structure of the undercurrent with laboratory experiments by Garcia (1993). Their observations reveal that the entrainment coefficients (C_E) are larger on steeper slopes and that the plume's gravitational forcing is responsible for its width expansion which is evident from the lateral structure of density anomaly and velocity.

The hydrodynamic structure of a turbulent jet from a river entering the receiving basins with different slopes, and its consequences on river mouth bar formation was studied by

Jiménez-Robles et al. (2016) using Delft3D. Their study showed that the entrainment coefficient shows a power lay increase with the slope of the receiving basin. Robles and Sanchez (2018) carried out a similar study using Delft3D, wherein they investigated the implications of the river discharge angle along with the basin slope on mouth bar morphology. Some studies like Siqueira et al. (2018) have also used Delft3D to investigate changes in sediment transport downstream of dams.

Recently, Ahmed et al. (2018) published a study that concerns the internal structure and the spatio-temporal evolution of a 3D density current in a miscible ambient fluid. They used RANS along with $(k-\epsilon)$ turbulence closure model and diffusion-convection equations to model the propagation and mixing of a saline gravity current. Their observations revealed that the mean density showed radial symmetry close to the inlet and asymmetry further away. Tseng and Chou (2018) used a nonhydrostatic three dimensional coastal model SUNTANS to study hyperpycnal plumes on sloping continental shelves. The nonhydrostatic simulations informed us about the detailed three dimensional flow structures. The nonhydrostatic effect is especially important for a plume that undergoes considerable changes and also where the slope increases. Tseng and Chou (2018) also observed that once the plume enters the continental slope, it begins to spread and the spread is weaker when the bed slope is steeper.

A.4 The Jet Integral Model

Early critical reviews show that many jet integral models had been proposed in the 1960s and 1970s, but with significant limitations and lacking some form of generalization (Jones et al., 2007). A new jet integral formulation for the buoyant surface discharge was developed by Jirka (2007) to provide for a detailed prediction of mixing in the near field region. The surface buoyant jet is formed by its initial fluxes of volume (Q_0), momentum (M_0) and buoyancy (B_0) given by

$$Q_0 = U_0 a_0 \tag{A.4}$$

$$M_0 = U_0^2 a_0, \tag{A.5}$$

$$J_0 = U_0 g_0' a_0 \tag{A.6}$$

where a_0 is the channel cross sectional area, U_0 is the average discharge velocity and $g_0' = (\Delta\rho_0/\rho_a)$ is the initial buoyant acceleration. The jet integral method and subsequent integration of all terms of the governing turbulent Reynolds equations of motion is explained in the work of Jirka (2007) which results in a system of simple ordinary differential equations. This integration results in the following integral quantities (bulk variables): (i) total volume flux within the turbulent zone (Q), (ii) axial momentum flux (M) (iii) buoyancy flux (J) and (iv) the tracer mass flux (Q_c)

$$Q = 2b_h b_v (a_{Q1} u_c + a_{Q2} u_a cos\sigma) \tag{A.7}$$

$$M = 2b_h b_v (a_{M1} u_c + a_{M2} u_a cos\sigma)^2 \tag{A.8}$$

$$J = 2b_h b_v (a_{S1} u_c + a_{S2} u_a cos\sigma) g_c' \tag{A.9}$$

$$O_c = 2b_h b_v (a_{S1} u_c + a_{S2} u_a cos\sigma) c_c \tag{A.10}$$

in which the coefficients $a_{Q1}, a_{Q2}, a_{M1}, a_{M2}, a_{S1}$, and a_{S2} are integration constants for discharge, momentum and scalars respectively. These coefficients are explained in detail in Jirka (2007) and all of them contain an exponential dependence on the Richardson number. As a result, for jet-like cases, the coefficients correspond to values for Gaussian profiles whereas for plume-like conditions, the values correspond to top-hat profiles.

Hetland (2010) studied the net change in density through the near-field plume, as a function of the channel mouth width and discharge and showed that the near-field plume behaves similar to an engineering-scale jet. He also stated that for such scenarios, the aspect ratio of the source (estuary/river) is important in determining the net dilution. To investigate such density changes, he introduced a simple layer model that includes plume spreading and entrainment. A buoyant fluid is introduced into a reservoir through a rectangular channel carved in a coast with width W_0. Setup of the layer model is similar to that as shown in Figure 2.10, where the outflow is steady, with a velocity u_0 and a density difference of $\Delta\rho_0$. A complete description about the development of the model can be found in Hetland (2010). Here, the width of the plume (W) needs to be solved.

Previous studies involving Hetland and MacDonald (2008) and Wright and Coleman (1974) have shown that the plume spreads with a rate proportional to the local internal gravity wave speed, $c = \sqrt{g'h}$ perpendicular to flow direction. Hence, the local rate of change in plume width is given by

$$\frac{DW}{Dt} = u\frac{\partial W}{\partial x} = 2\sqrt{g'h} \tag{A.11}$$

The factor 2 is required as the plume spreads along both edges. It is assumed that the plume front expands in the along-shore direction at the local internal gravity wave speed. The model is based on a 1-D, steady and layer averaged governing equations for conservation of fluid mass, volume, and momentum. It also assumes that vertical and lateral velocities are negligible, that the Boussinesq approximation holds, and that the flow and scalar quantities can be described using top-hat profiles (Strom and Keyvani, 2016). Hence, under the stated assumptions, the model reduces to the following system of ordinary differential equations

$$\frac{\partial \Delta\rho}{\partial x} = -\Delta\rho\frac{w_e}{uh} \tag{A.12}$$

$$\frac{\partial W}{\partial x} = 2F_r^{-1} \tag{A.13}$$

$$\frac{\partial u}{\partial x} = \frac{u}{(1 - F_r^{-2)}}[\frac{1}{\Delta\rho}\frac{\partial \Delta\rho}{\partial x} + F_r^{-2}\frac{1}{W}\frac{\partial W}{\partial x}] \tag{A.14}$$

$$\frac{\partial h}{\partial x} = -h[\frac{1}{\Delta\rho}\frac{\partial \Delta\rho}{\partial x} + \frac{1}{W}\frac{\partial W}{\partial x} + \frac{1}{u}\frac{\partial u}{\partial x}] \tag{A.15}$$

where w_e is the entrainment velocity of ambient fluid that represents mixing of density and momentum from the lower layer to the upper layer. The solutions to this set of equations is valid only for supercritical flow ($F_r > 1$). Hetland and MacDonald (2008) showed that plume properties are a function of the radial distance (r)from the river mouth. However, these equations are expressed in terms of the independent variable x as there are no derivatives in the transverse (cross-shore) direction.

A.5 Plume Width Definitions

Many studies like Wright and Coleman (1971) calculate plume widths based on visual boundary observed through images. In the case of MacDonald and Geyer (2004), they calculated plume width from

$$Q_0 = \int_{z_{S0}}^{0} u\frac{(S_0 - S)}{S_0} b dz \tag{A.16}$$

where Q_0 is the total fresh water flux in the cross section which is a constant, u is the velocity parallel to the flow direction (defined as the x direction), S is the local salinity and $b = b(x, z)$ is the plume width in the cross stream direction. Using this same concept, MacDonald et al. (2007) calculated the width expansion of the plume in the seaward direction. Hetland and MacDonald (2008) and Chen et al. (2009) make use of streamlines, particle tracers and introduce numerical drifters in their simulations to track their paths and calculate plume width as the distance between streamlines or particle tracks. Kilcher et al. (2012) estimated the lateral spreading of plume width by using the principle of conservation of freshwater flux along the transect.

Yuan and Horner-Devine (2013) dyed the freshwater with colored food dye and the plume thickness (h_e) was measured using the Optical Thickness Method (OTM). A centered nonnormalized Gaussian fit was successful in describing the lateral distribution of (h_e) at each location along the plume axis and the plume width b was defined in terms of the standard deviation of the Gaussian fit $b = 4\sigma$.

For a hyperpycnal case, the study of Chen et al. (2013) used a passive tracer to distinguish plume water from ambient water. The tracer concentration is unity in the river and is zero elsewhere. They normalize the local maxima at each alongshore section to account for dilution due to entrainment and the plume boundary is marked using a cutoff of the normalized concentration. They found that using different values of cutoff concentrations gave similar results. The plume cross sectional area (A), layer thickness (H) and width (W) is then calculated as

$$A = \int\int M dz dy \tag{A.17}$$

$$H = \int M dz \tag{A.18}$$

$$W = \frac{A}{H} \tag{A.19}$$

where M is the mask for tracer concentration, unity where the concentration is greater than the cutoff value and zero elsewhere.

The literature indicates that density plumes, in an unconfined domain, spread laterally in the alongshore direction. A majority of this work centered on hypopycnal plumes, some laterally confined hyperpycnal plumes, determination of their plunge location and establishing its relationship with the densimetric Froude number at plunge. Some studies also focused on quantifying the spread in a buoyant plume. That said, the spreading of a plume with a hyperpycnal potential is still relatively untouched. Furthermore, little work has been done to quantify the spreading and its affect on the plunging of flows under different domain characteristics.

Appendix B

Additional Plots

B.1 Spreading

As mentioned in Section 4.5, the rate of plume spreading shows similar trends with Richardson number. Figure 4.8 serves as an example that shows results for one simulation (scenario 1, $C_z = 45$). Plots for rest of the scenarios and friction factors are given below:

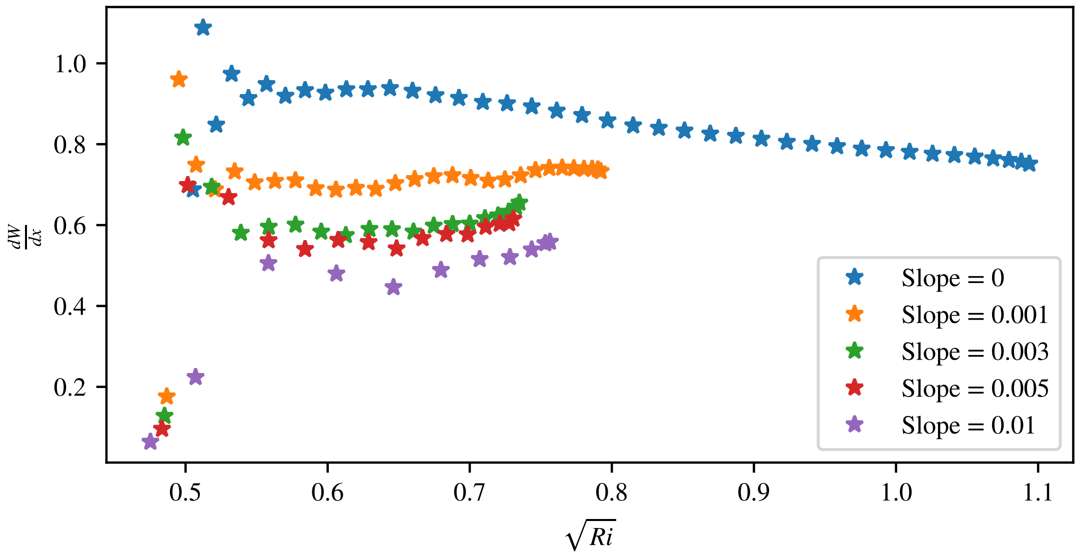

Figure B.1: dW/dx for Scenario 1 ($C_z = 55$)

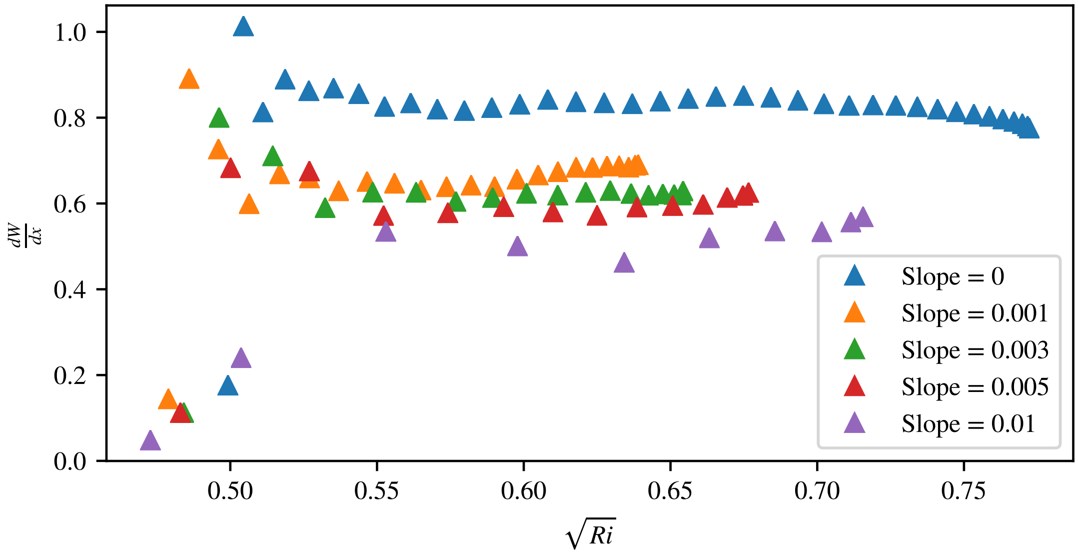

Figure B.2: dW/dx for Scenario 1 ($C_z = 65$)

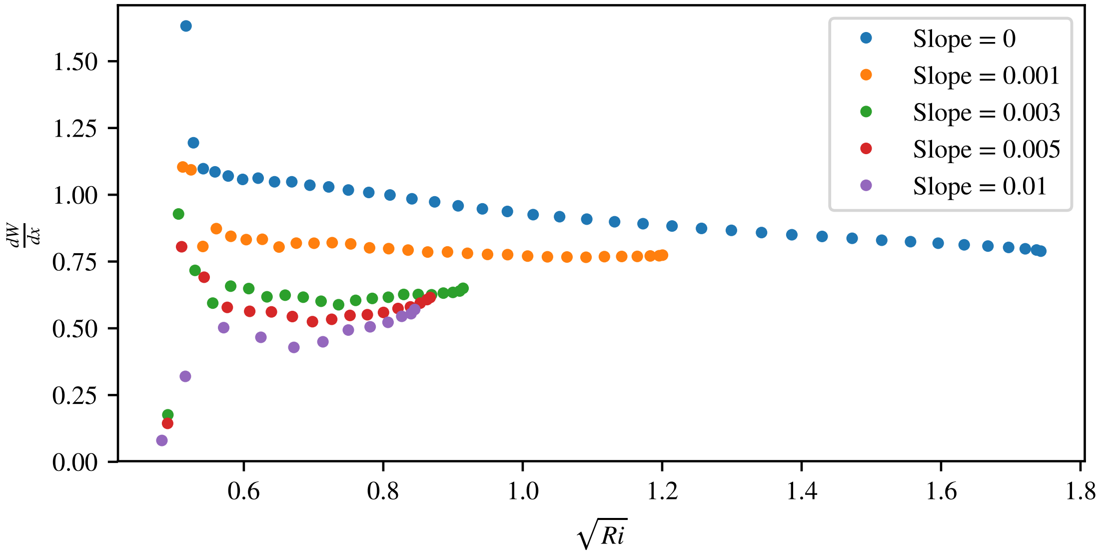

Figure B.3: dW/dx for Scenario 2 ($C_z = 45$)

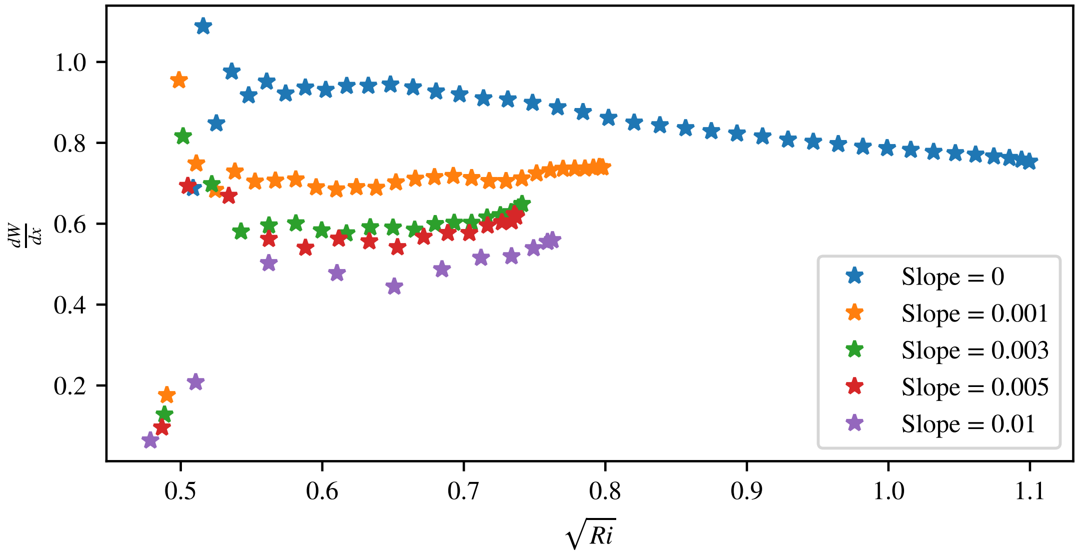

Figure B.4: dW/dx for Scenario 2 ($C_z = 55$)

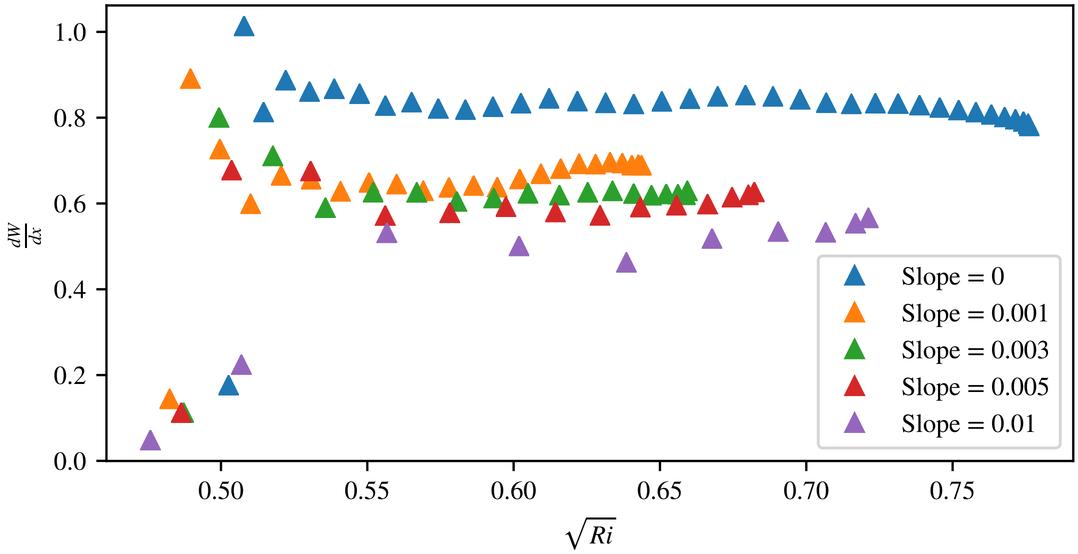

Figure B.5: dW/dx for Scenario 2 ($C_z = 65$)

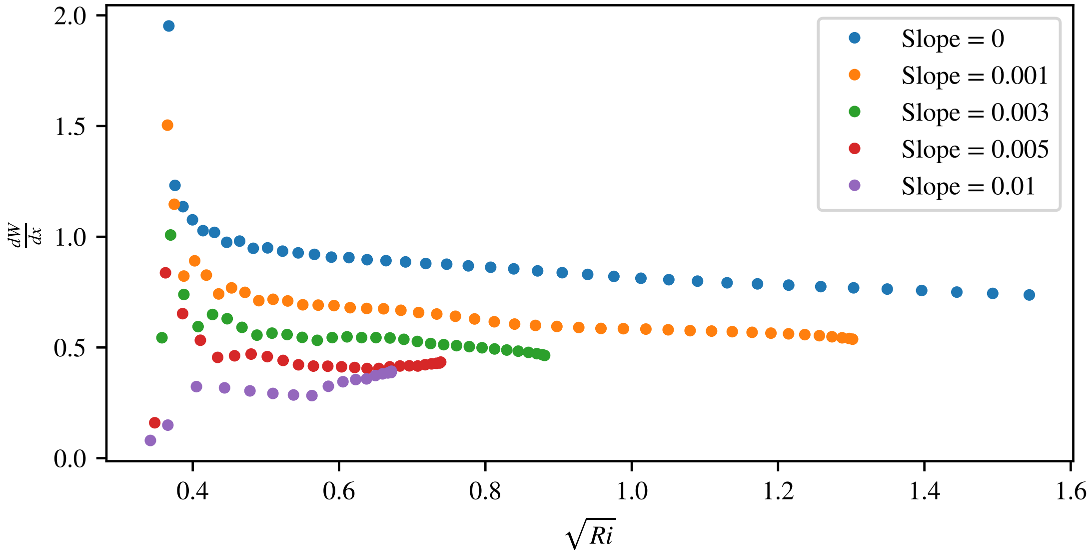

Figure B.6: dW/dx for Scenario 3 ($C_z = 45$)

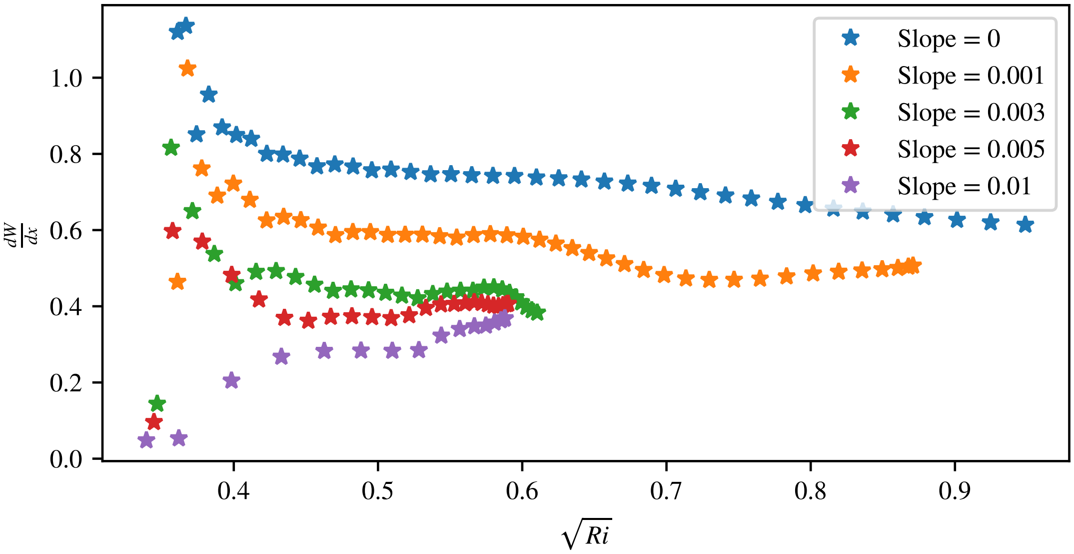

Figure B.7: dW/dx for Scenario 3 ($C_z = 55$)

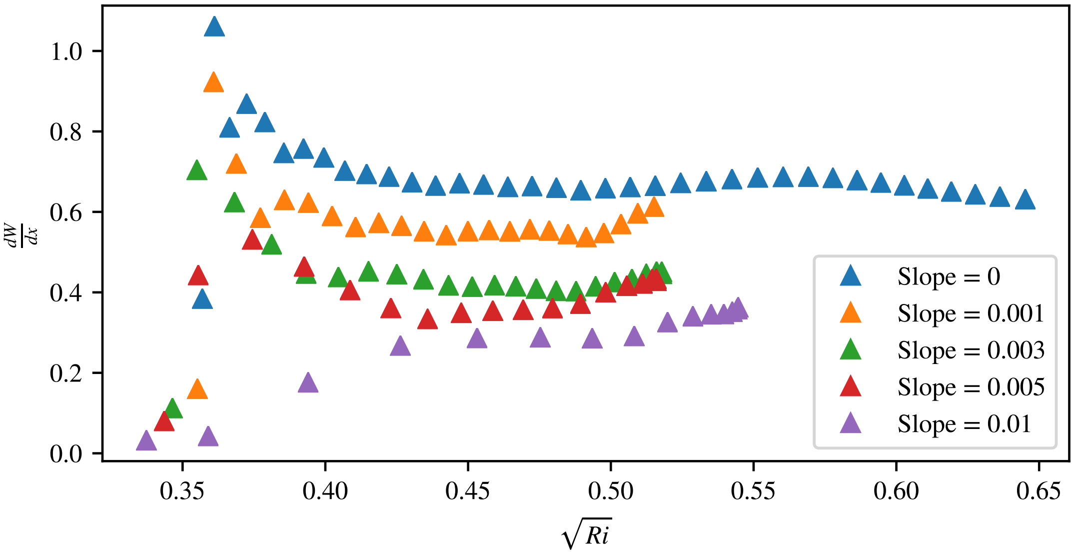

Figure B.8: dW/dx for Scenario 3 ($C_z = 65$)